C. RESULTS

C.1. miRNAs used in this work

Our group has focused on the regulation and function of the *let-7* miRNA in the nervous system. In humans and mice the *let-7* family consists of 12 precursor genes (including the highly related *mir-98*) that encode nine distinct, mature 22 nt sequences. Examples of ~70 nt precursor stem-loop structures are shown in Figure C.1 A. The mature forms (designated *let-7a* through *let-7i*) differ at one to four positions from the canonical *let-7a* sequence (Figure C.1 B).

A.

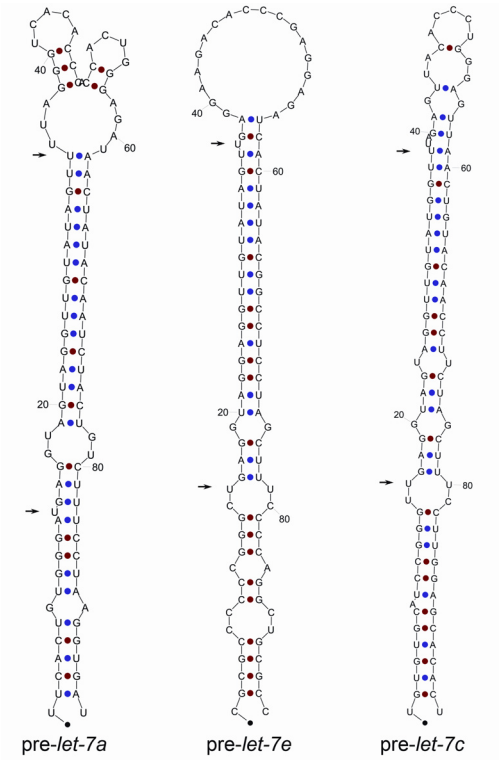

B.

let-7 Family	Sequence	Chromosome
let-7_Ce:	UGAGGUAGUAGGUUGUAUAGUU	X
let-7a_Mm:	UGAGGUAGUAGGUUGUAUAGUU	9; 13
let-7b_Mm:	UGAGGUAGUAGGUUGUGUGGUU	15
let-7c_Mm:	UGAGGUAGUAGGUUGUAUGGUU	15; 16
let-7d_Mm:	AGAGGUAGUAGGUUGCAUAGU	13
let-7e_Mm:	UGAGGUAGGAGGUUGUAUAGU	17
let-7f_Mm:	UGAGGUAGUAGAUUGUAUAGU	13
let-7g_Mm:	UGAGGUAGUAGUUUGUACAGU	9
let-7i_Mm:	UGAGGUAGUAGUUUGUGCUGU	10
mir-98_Mm:	UGAGGUAGUAAGUUGUAUUGUU	X

Figure C.1. Stem-loop precursors and mature *let-7* family sequences. **Panel A:** stem-loop precursor structures of Mus musculus pre-*let-7a*, pre-*let-7e*, pre-*let-7c*). The mature forms of miRNAs are shown with arrows. Folding of miRNA precursors was performed with MFOLD Web Server (http://www.bioinfo.rpi.edu/applications/mfold/rna/form1.cgi). **Panel B:** The sequences of mouse *let-7* family members in comparison to *C. elegans let-7* sequence (*let-7_Ce*). Identical nucleotides are shaded with grey. Localization in genome is shown to the right. Ce – *C. elegans*; Mm – Mus musculus.

In addition to *let-7* family, other mouse brain-specific or brain-enriched miRNAs were analyzed in this work. Their sequences are listed in Table C.1.

Table C.1. miRNA Sequences

miRNA name	miRNA sequence
mmu-let-7a	UGAGGUAGUAGGUUGUAUAGUU
mmu-let-7c	UGAGGUAGUAGGUUGUAUGGUU
mmu-let-7e	UGAGGUAGGAGGUUGUAUAGU
mmu-mir-124b	UUAAGGCACGCGGGAGAAUGC
mmu-mir-125b	UCCCUGAGACCCUAACUUGUGA
mmu-mir-128a	UCACAGUGAACCGGUCUCUUUU
mmu-mir-23a	AUCACAUUGCCAGGGAUUUCC
mmu-mir26a	UUCAAGUAAUCCAGGAUAGGC
mmu-mir26b	UUCAAGUAAUUCAGGAUAGGUU
mmu-mir-29b	UAGCACCAUUUGAAAUCAGUGUU
mmu-mir-29c	UAGCACCAUUUGAAAUCGGU
mmu-mir-294	AAAGUGCUUCCCUUUUGUGUGU
mmu-mir9	UCUUUGGUUAUCUAGCUGUAUG

C.2. miRNA expression during neural development

C.2.1. Temporal expression of neural miRNAs during mouse brain development

Temporal regulation of miRNA expression is critical in the genetic pathways controlled by both *lin-4* and *let-7* in *C. elegans*. Therefore the studies were begun by examining temporal expression of *let-7* and other neural miRNAs throughout the course of mouse brain development. A developmental Northern blot was prepared with RNA samples isolated from embryonic Day 12 to postnatal Day 0 (Figure C.2 A). A second blot covered the early postnatal period from P3 to P14. For comparison RNA from the cerebellum was prepared separately from the remaining cortex and midbrain (Figure C.2 B). The probes for Northern blot analysis included the following miRNAs: three *let-7*-family members (*let-7a*, *let-7c*, and *let-7e*) and a set of miRNAs (*mir125b*, a homolog of *lin-4*, *mir-9*, *mir-23*, *mir-124*, *mir-128*, *mir-26*, *mir-29*) with strong expression in the adult mouse brain, based on their representation in expression libraries [28]. The results are presented in Figure C.2 A and B. Each of the *let-7* miRNAs was expressed at low levels prior to E14. Expression of *let-7a* and *let-7c* increased rapidly until E17 and leveled off thereafter. *let-7e* induction was less steep and peaked at E15. All three *let-7* forms declined in the perinatal cerebral cortex, but increased in the cerebellum. As judged by signal strength, *mir-26*, *mir-124* and *mir-128* were the most strongly expressed miRNAs tested. *mir-23* and *mir-26* were expressed at fairly constant levels throughout the time period covered in this experiment. *mir-9*, *mir-125* and *mir-128* were initially expressed at low levels that increased continuously during embryonic development. *mir-125* was unique in showing a gradual post-natal decline in expression. Levels of all other miRNAs declined only minimally from their individual peaks. Induction of *mir-124* was biphasic, with peaks at E14 and E17 and very strong postnatal expression. *mir-29* expression was minimal throughout the

embryonic and perinatal periods, expression did not commence until P14. From these results, it is clear that individual neural miRNAs have distinct patterns of temporal expression.

In addition to the mature miRNAs, cytoplasmic ~70 nt precursor forms were also detected with *let-7a*, *let-7c*, *let-7e*, *mir-9* and *mir-124* probes. In contrast to the mature forms, precursor forms were expressed at essentially constant levels over the course of development.

The difference in temporal regulation between mature and precursor forms apparent in the Northern blots suggested an element of post-transcriptional control in the regulation of miRNA expression. This was further investigated by examining the expression profile of the primary nuclear miRNA transcripts. RT-PCR was performed on total RNA from selected time points from E13 to P14 for primary transcripts of the *let-7a-1* and *let-7f-1* pair from chromosome 13 (pri-*let-7a*), and a cluster of three miRNAs from chromosome 17 containing *mir-99b*, *let-7e* and *mir-125a* (pri-*let-7e*). Primary transcripts were detected in cDNA from each of five time points sampled, but not in mock cDNA prepared without addition of reverse transcriptase (Figure C.3). The expression profile was relatively flat, with a modest increase between E16 and P0 compared to E13, similar to the constitutive precursor expression detected by Northern blots. The lack of strong transcriptional upregulation of primary and precursor miRNAs compared to the massive accumulation of mature miRNAs suggested a significant contribution from posttranscriptional mechanisms.

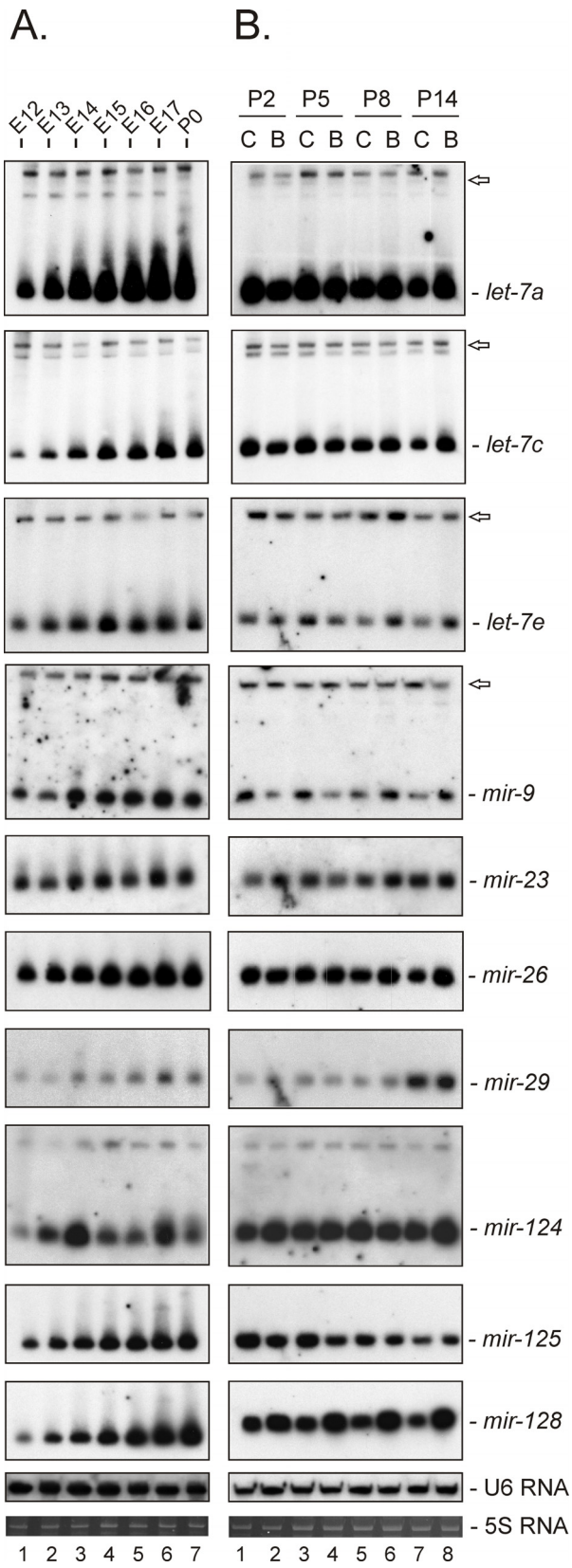

Figure C.2. Northern blot analysis of neural miRNA expression during mouse brain development. **Panel A:** Total RNA was isolated from neural tissue representing embryonic Days 12 to 17 (E12-E17, **Lanes 1-6**) and post-natal Day 0 (P0, **Lane 7**). For miRNAs with clear precursor expression, the portion of the filter corresponding to ~80 nt is shown. The gel was stained with EtBr prior to transfer. The U6 and 5S RNA bands are shown in the last two panels as controls for equal loading. **Panel B:** miRNA expression during early postnatal development. RNA from the cerebellum (B) was prepared separately from the remaining tissue, including midbrain, basal ganglia and cerebral cortex (denoted C) as indicated above each lane. Developmental stage for each pair P2, P5, P8 and P14 is indicated. Images were cropped to show all specific signals obtained with each probe. Precursor forms are marked by an arrow.

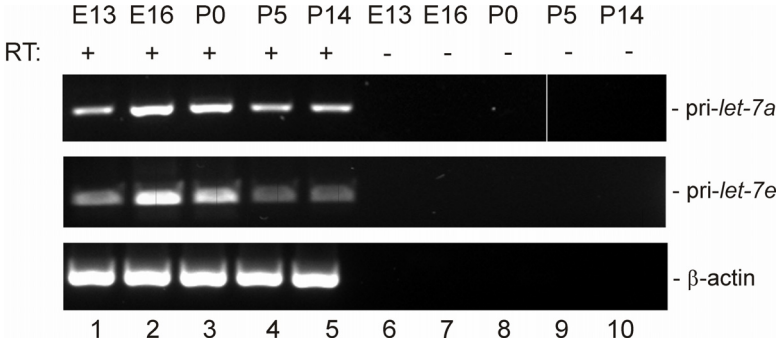

Figure C.3. Expression of primary nuclear *let-7* miRNAs transcripts in mouse brain development. RT-PCR was performed on total RNA from selected time points from E13 to P14. Primary transcripts were amplified with primers specific for *let-7a-1/let-7f-1* (pri-*let-7a*) or *mir-99/let-7e/mir-125a* (pri-*let-7e*) (**Lanes 1-5**). Control reactions were performed on mock cDNA prepared without addition of reverse transcriptase (RT) (**Lanes 6-10)**. cDNA integrity was monitored using primers specific for β-actin.

C.2.2. Lineage specificity of miRNA expression in primary neurons and astrocytes.

In order to investigate cell specificity of miRNA expression, RNA from primary cultures of embryonic cortical neurons (E17) and perinatal astrocytes (P3) were used for Northern blot analysis. For comparison, RNA from total brain (E15) and from differentiated P19 EC cells was run in parallel. EC cells were treated with RA to induce differentiation of neuronal and glial cell types (see Materials and Methods, Section B.2.1.1), RNA was collected at Day 12 after induction. Individual miRNAs showed strong lineage specificity in this experiment (Figure C.4). Whereas *mir-23* expression was observed almost exclusively in astrocytes, *mir-124* and *mir-128* were tightly restricted to neurons. *let-7a*, *let-7c let-7e* and *mir-125* were preferentially expressed in neurons. For each miRNA, the level of expression in cultured primary cells was similar to that seen in total brain RNA from E15. As a control for RNA integrity, the blot was hybridized with U6 RNA (Figure C.4, bottom panel). Seventy nucleotide precursor forms were also detected with *let-7c* and *let-7e.* There was a clear disparity between accumulation of the precursor and mature forms, as pre-miRNAs were expressed at similar levels in primary neurons and astrocytes, while mature miRNAs were restricted to primary neurons.

To address the question of regulation of miRNA expression, the levels of the primary transcripts (pri-*let-7a* and pri-*let-7e*) were compared by RT-PCR. Despite the differential expression of the mature miRNAs, primary transcript levels were similar (Figure C.5). This result was confirmed by Real-Time PCR. The degree of transcriptional activity for *let-7a* or *let-7e* was similar in both cell types (data not shown).

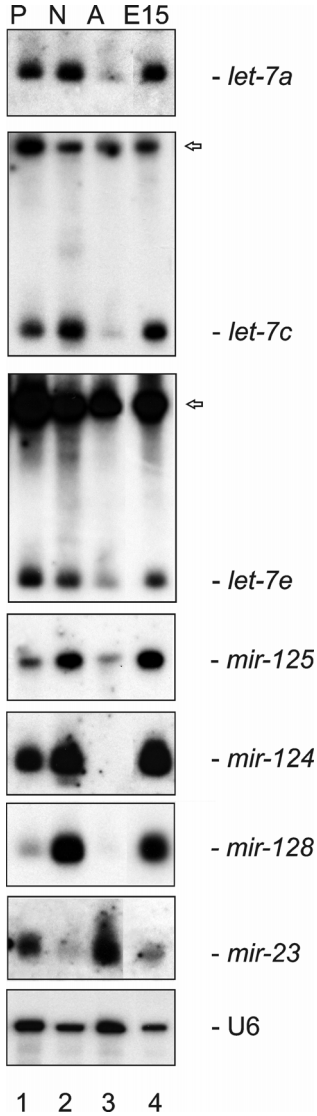

Figure C.4. miRNA expression in primary embryonic neurons and astrocytes. The ~22 nt region of a Northern blot probed for the miRNA indicated to the right of each exposure is shown. RNA was isolated from P19 EC cells 12 days after stimulation with RA (P, **Lane 1)**; primary neurons (N, **Lane 2**); primary astrocytes (A, **Lane 3**); and for comparison E15 total brain RNA (E15, **Lane 4**). For miRNAs with clear precursor expression, the portion of the filter corresponding to ~80 nt is shown. Precursors are indicated with an arrow. As a control for RNA integrity and transfer the filter was hybridized with a probe against U6 RNA (bottom panel).

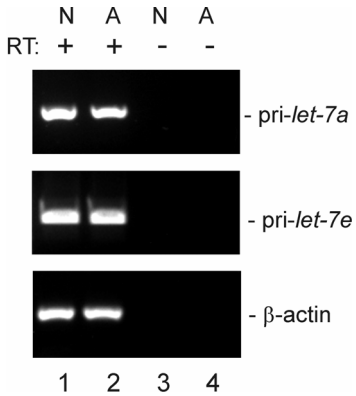

Figure C.5. Expression of primary *let-7* miRNA transcripts in embryonic neurons (N, **Lanes 1** and **3**) and astrocytes (A, **Lanes 2** and **4**). Poly-dT primed cDNAs were amplified with primers specific for *let-7a-1/let-7f-1* (pri-*let-7a*) or *mir-99/let-7e/mir-125a* (pri-*let-7e*) (**Lanes 1** and **2**). Control reactions with mock cDNA are shown in **Lanes 3** and **4**. cDNA integrity was monitored using primers specific for β-actin.

These results strongly suggest that miRNA expression in the mammalian CNS is lineage-specific. To further investigate this result, the effects of cell growth and maturation in culture were evaluated in E17 cortical cells. Starting from pooled cells, one half was used to culture neurons and the other half to culture astrocytes. RNA was isolated one week and three weeks after initial plating. The results are shown in Figure C.6. miRNAs fell into three groups: one exclusively neuronal (*mir-124*, *mir-128*), a second strongly astrocytic (*mir-23*, *mir-29*), and a third with mixed expression (*mir-9*, *mir-26* and *mir-125*). The expression of mature *mir-9* was close to the detection limit despite pronounced precursor expression. miRNA expression decreased as a function of time in culture for neurons, but increased for astrocytes. For both *mir-9* and *mir-125* it is interesting to note that the ratio of ~70 nt precursor to mature miRNA was higher in astrocytes compared to neurons, suggesting differences in miRNA maturation between the two cell types.

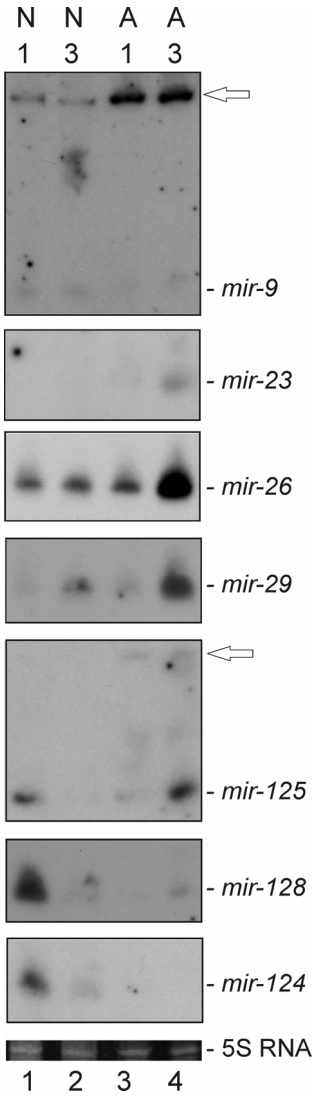

Figure C.6. Northern blot showing miRNA expression in primary neurons and astrocytes during cultivation. E17 neurons (N, **Lanes 1 and 2**) and astrocytes (A, **Lanes 3 and 4**) were maintained for either one week (**Lanes 1 and 3**) or three weeks (**Lanes 2 and 4**) in culture prior to isolation of RNA. Hybridization probes are indicated to the right; when detected, the position of precursor forms is denoted by an arrow. 5S RNA stained with ethidium bromide is shown in the bottom panel as control for equal loading.

C.2.3. Temporal expression of neural miRNAs during ES cell and EC cell differentiation

Examination of the kinetics of induction in the mouse developmental Northern blots suggests that expression levels prior to E12, the earliest practicable time point for analysis, are quite low and that the ratio of precursor to mature RNA is high (see Figure C.2 A). Moreover, the results obtained with brain samples and particularly in primary cells suggested that the accumulation of mature miRNA may be subject to regulation at steps subsequent to the transcription of the primary transcript. To study early regulation of the primary transcript, precursor and mature forms two well-established model systems were applied: neural differentiation of ES cells and P19 EC cells. ES cells were cultured as EBs and treated with RA, an inducer of neuronal and glial cell phenotypes. At Day 5 of the induction EBs were plated. RNA was isolated on Day 12 and Day 24. With this protocol, cell numbers staining positively for neuron-specific markers peak by Day 12. Thereafter, neurons mature phenotypically, and $GFAP^+$ cells begin to accumulate. miRNA levels during ES neural differentiation were monitored by Northern blot analysis. The results are presented in Figure C.7.

With the exception of *mir-294*, a miRNA specifically expressed in undifferentiated ES cells and EBs and included as a control for RNA integrity [34], none of the miRNAs examined could be detected in RNA isolated from undifferentiated ES cells (U, - RA). Nevertheless, in the case of the *let-7* family members *let-7c* and *let-7e*, ~70 nt hybridization signals corresponding to the cytoplasmic precursor forms were detected. All of the miRNAs tested were induced during the course of neural differentiation, and in most cases the level of expression attained was comparable to that of embryonic brain at E15 (Figure C.7, lane 4). Interestingly, induction of *mir-124* was transient, with signal readily apparent at Day 12 but below detection at Day 24. A similar pattern was observed with *mir-9*, but at expression levels close to the detection limit (not shown). To test if the cell specificity of miRNA expression observed in Northern blots with tissue samples is maintained in the ES cell model, expression of *let-7*, *mir-23*, *mir-125* and *mir-128* was compared between protocols favoring cardiomyocyte (induction of differentiation in the absence of exogenous inducer) or neural differentiation (induction with RA). RNA from cells maintained as EBs for seven days in the absence of chemical inducer was also examined (Figure C.8). The expression of each of the miRNA increased in response to differentiation. *mir-23* showed the earliest expression with a weak signal apparent at the EB stage (Figure C.8, Lane 2). Each of the miRNA was more strongly expressed in the neural culture (D + RA) in comparison to cardiomyocyte differentiation (D - RA), with differential expression of *mir-23* the most pronounced.

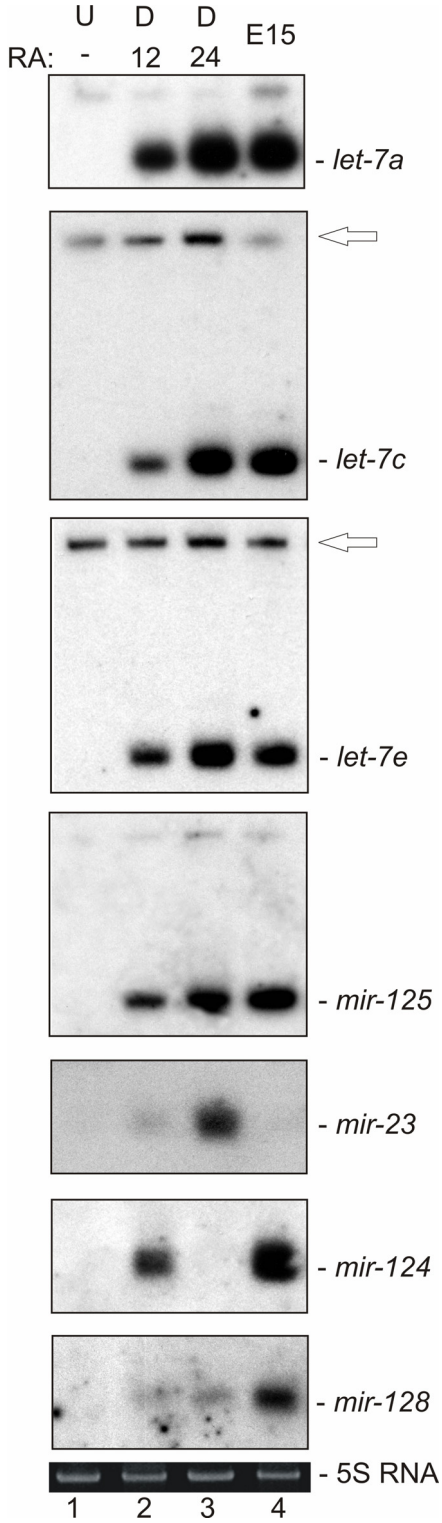

Figure C.7. miRNA induction during *in vitro* neural differentiation of ES cells. Total RNA was prepared from ES cells cultured in the differentiation inhibitor LIF at Day 0 (U, RA-, **Lane 1**); 12 days after RA treatment (D, RA-12, **Lane 2**); 24 days after RA treatment (D, RA-24, **Lane 3**); and from E15 total brain RNA (E15, **Lane 4**) as control. Refer to Materials and Methods for details of cellular differentiation (Section B.2.1.2). The ~22 nt miRNA signal is indicated to the right. The hybridization signal for those miRNA displaying precursor expression is marked by an arrow.

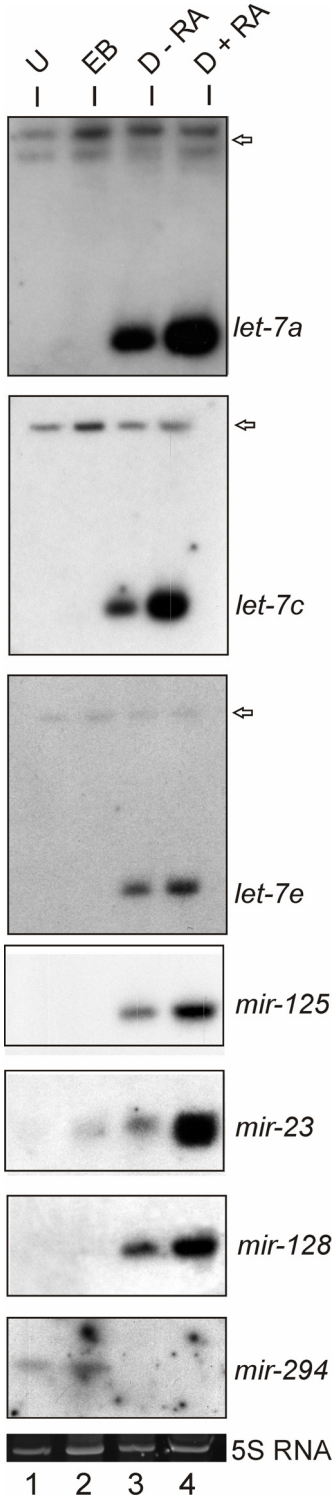

Figure C.8. Northern blot showing comparison of miRNA induction in EB, cardiomyocyte and neural ES cell preparations. RNA was isolated from undifferentiated ES cells cultured in the presence of LIF (U, **Lane 1**); after cultivation for seven days as EB (EB, **Lane 2**); on Day 13 of cardiomyocyte differentiation (D-RA, **Lane 3**); or Day 24 after induction of neural differentiation by RA (D+RA, **Lane 4**) (see Materials and Methods for details). Images were cropped to show all specific signals obtained with each probe. Precursor forms are marked by an arrow.

As noted above, hybridization signals representing ~70 nt cytoplasmic precursor forms of *let-7* family members were clearly detected in both undifferentiated as well as differentiated cell samples (Figure C.8). Precursors were detected at approximately equal levels in all four lanes. To verify probe specificity, all results obtained with DNA probes were confirmed using LNA probes.

In multiple experiments, the precursor bands detected with the individual probes could be distinguished on the basis of mobility, consistent with predicted precursor lengths as generated by Drosha cleavage (ranging from 66 nt for *let-7e*, 69 nt for *let-7c-2* and 72 nt for *let-7a-1*). These results demonstrate that the hybridization conditions can distinguish between related pre-*let-7* molecules.

To confirm the results obtained with ES cells, a similar experiment with P19 EC cells was performed. EC cells were incubated as EBs with RA for 4 days to induce neural differentiation. After 4 days of induction, RA was removed; EBs were resuspended and plated in cell culture dish. After 3 days medium was changed to Neurobasal Medium supplemented with B27. RNA was isolated 12 days after induction of differentiation. A Northern blot was probed for *let-7a, let-7c* and *let-7e*, *mir-9, mir-125b, mir-124, mir-128, mir-23*, and for U6 RNA as a control of equal loading. (Figure C.9). Whereas accumulation of mature *let-7* and *mir-9* forms was dependent on cell differentiation, each precursor molecule was readily detected in undifferentiated (U) as well as in differentiated (D) samples. The expression of *mir-125b, mir-124, mir-128* was restricted to differentiated EC cells (D). *mir-23* showed the earliest expression with a weak signal apparent in the undifferentiated cells.

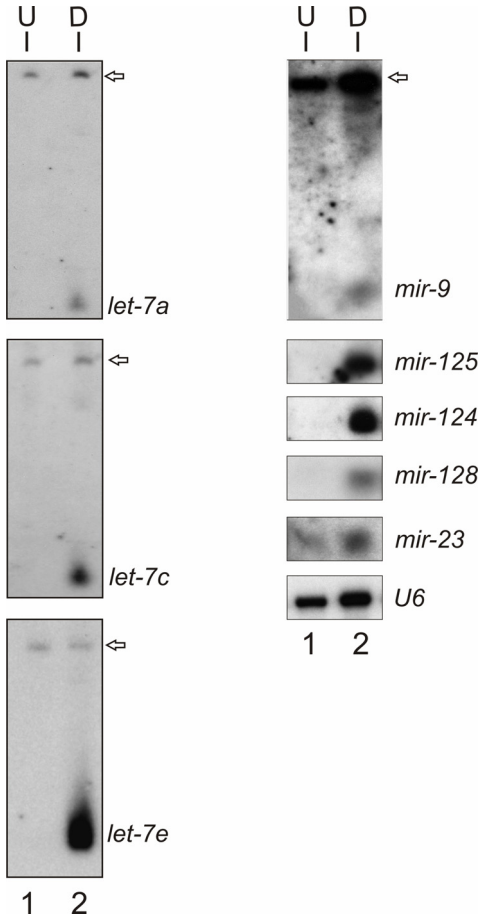

Figure C.9. miRNA induction during *in vitro* differentiation of P19 EC cells. Total RNA was prepared from undifferentiated EC cells at Day 0 (U, **Lane 1**); or 12 days after RA treatment (D, **Lane 2**). Precursor forms are indicated by an arrow to the right.

As a next step primary transcripts were assayed, again comparing undifferentiated and differentiated ES and EC cells. RT-PCR was performed to amplify pri-*let-7a* and pri-*let-7e* transcripts. The quality of the cDNAs used and the stringency of the differentiation protocol were monitored using primers specific for the alternatively spliced α6-integrin mRNA (Figure C.10 A and B). As expected, undifferentiated cells predominantly expressed a characteristic short α6-integrin isoform. Differentiation was accompanied by an efficient switch to a longer isoform. Primary transcripts from the two *let-7* loci were readily detected in both undifferentiated and differentiated cells, consistent with the constitutive expression of the hairpin precursor observed in Northern blots. As a control, no product was observed in reactions using mock cDNAs (-RT). The degree of transcriptional activation was quantified by Real-Time PCR using GAPDH as a standard. Levels of pri-*let-7e* were 4- and 7-fold higher and levels of pri-*let-7a* 6- and 10-fold higher after differentiation in ES and EC cells, respectively. From this result, it appears that transcriptional activation contributes to the burst of *let-7* expression during differentiation, although the degree of activation may not be sufficient to account for the full magnitude of the induction. Furthermore, the consistent detection of the primary transcript in undifferentiated cells suggests that the lack of mature miRNA in these cells is most likely due to a post-transcriptional mechanism.

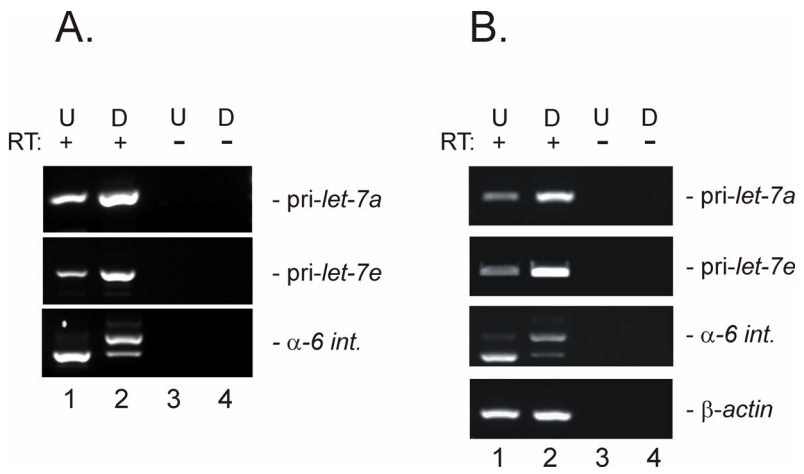

Figure C.10. Expression of primary *let-7* transcripts in undifferentiated (U, **Lanes 1** and **3**) and differentiated (D, **Lanes 2** and **4**) EC (**Panels A)** and ES **(Panel B)** cells. Poly-dT primed cDNAs were amplified with primers specific for *let-7a-1/let-7f-1* (pri-*let-7a*) or *mir-99/let-7e/mir-125a* (pri-*let-7e*). For both miRNA clusters, differentiation was accompanied by a modest increase in the level of primary transcripts. Differentiation was monitored using the pattern of α6-integrin transcripts. Undifferentiated cells exclusively expressed the characteristic short isoform (**Lane 1**). In differentiated cells alternative splicing generates a long transcript as predominant isoform (**Lane 2**). Control reactions with mock cDNA are shown in **Lanes 3** and **4**.

During the course of this work Kim and co-workers demonstrated that RNA polymerase II is responsible for the initial, primary miRNA transcripts [39]. This finding allowed the use of the chromatin immunoprecipitation (ChIP) technique to assay for transcriptional activity of *let-7* genes. In this assay, chromatin was cross-linked to associated proteins and then fractionated. The resulting

complexes were immunoprecipitated with a pol II-specific antibody; after elution coprecipitated DNA was amplified with primers corresponding to the pri-*let-7a* and pri-*let-7e* transcripts. As shown in Figure C.11, the efficiency of product amplification was similar in immunoprecipitates from undifferentiated (U) and differentiated (D) cells, confirming active *let-7* transcription in undifferentiated cells. This result suggests that specific association of pol II with each *let-7* cluster was independent of the cellular differentiation state. In RA-treated P19 EC cells the Oct4 promoter is subject to negative regulation by RA [150]. Therefore, as a control, transcriptional downregulation of the Oct4 marker following differentiation was verified in samples processed in parallel.

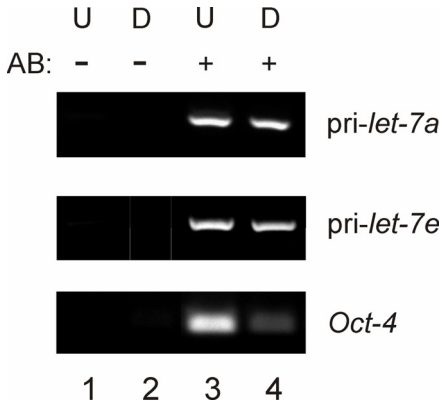

Figure C.11. ChIP assay for pri-*let-7e,* pri-*let-7e* and Oct4. DNA eluted from precipitates obtained with or without anti-RNA pol II antibody (AB – or +), as indicated above each lane, was amplified with specific primers for pri-*let-7* transcripts or Oct4 as indicated to the right. Specific association of pol II with each *let-7* cluster was independent of differentiation state (compare **Lanes 3** and **4**). As expected, Oct4 transcription was significantly diminished in differentiated cells (D, **Lane 4**).

C.2.4. Screening of the additional cell lines for miRNA expression

To screen for additional cell models, we examined a panel of cell lines including HT-22 (neurons), U373 (astrocyte) and BV-2 (microglia), in comparison to primary cells and ES cells (Figure C.12). For several miRNAs with strong representation in brain libraries (*let-7a*, *mir-125* and *mir-128*) expression levels in cell lines were found to be low compared to either primary neurons or differentiated ES cells. Expression levels of *let-7a, mir-125* and *mir128* in cell lines were 5-fold lower than in ES cells or neurons. In contrast, *mir-23* was expressed in each of the cell lines tested, as well as in stem cell-derived neurons, but was negligible in primary neurons and astrocytes. A summary of miRNA expression patterns, described in Section C.2, is presented in Table C.2.

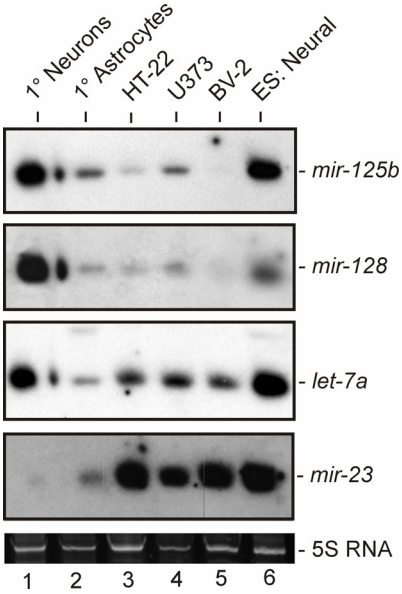

Figure C.12. miRNA expression in primary neurons, astrocytes and selected cell lines. The ~22 nt region of a Northern blot probed for the miRNAs indicated to the right of each exposure is shown. RNA was isolated from primary neurons (**Lane 1**); primary astrocytes (**Lane 2**); HT-22 cell line (**Lane 3**); U373 cell line (**Lane 4**); BV-2 cell line (**Lane 5**); and for comparison ES cells 24 days after RA treatment (**Lane 6**). **Lane 1** is distorted by a tear in the gel prior to transfer that does not affect the results. As a control, ethidium bromide staining of 5S RNA in the gel prior to transfer is shown in the last panel.

Table C.2. Summary of miRNA expression data. Data are compiled from Figure C.4, Figure C.6, Figure C.7, Figure C.8 and Figure C.9. Abbreviations: P.N. – primary neurons, P.A. – primary astrocytes, U – undifferentiated, EB – embryoid body, D12 and D24 – 12 and 24 days after differentiation with RA. "– " – miRNA is not expressed; "-/+" – miRNA is expressed on the detection limit; "+", "++" – miRNA is expressed; "+++" – very strong expression level of miRNA; NA – not assayed.

miRNA	P.N.	P.A.	P19 EC cells		ES cells			
			U	D 12	U	EB	D 12	D 24
mir-9	-/+	-/+	-	-/+	-		-/+	-
mir-23	-	+	-/+	++	-	+	+	++
mir-26	+	+++	NA	NA	NA	NA	NA	NA
mir-29	-/+	+++	NA	NA	NA	NA	NA	NA
mir-124	+++	-	-	+++	-	-	+	-
mir-125	+++	+	-	+++	-	-	+	++
mir-128	+++	-	-	+	-	-	-/+	+
mir-294	NA	NA	NA	NA	+	+	-	-
let-7a	+++	-/+	-	+	-	-	+	++
let-7c	+++	-/+	-	++	-	-	+	++
let-7e	+	-/+	-	+++	-	-	+	++

Analyzing the results from Section C.2 it can be concluded that individual miRNA genes display distinct temporal expression patterns and cell-type specificity. Moreover, comparison of primary, precursor and mature miRNA levels during embryonic brain development as well as neural differentiation of ES and EC cells suggests post-transcriptional regulation of miRNA accumulation.

C.3. miRNA processing

C.3.1. Developmental regulation of miRNA processing activity

The investigations presented thus far revealed differential regulation of miRNA expression, in terms of both lineage and temporal specificity. In particular, the disparity in expression between primary transcripts and precursor miRNA forms on the one hand, and mature miRNA forms on the other hand, as observed by Northern blotting, RT-PCR and ChIP assays in ES and EC cells, strongly suggested that accumulation of the mature, 22 nt miRNA during differentiation is subject to post-transcriptional regulation. A number of possible molecular mechanisms could be invoked to account for these observations, including altered cellular compartmentalization, turnover and/or precursor processing. Of these, developmental regulation of the processing pathway appeared most likely, and was amenable to direct biochemical analysis. Therefore, miRNA processing activity was examined as a function of differentiation state using an *in vitro* miRNA processing assay.

The *mir-30* precursor RNA (pre-*mir-30*) was used as a substrate for initial experiments, because pre-*mir-30* has been used in several previous studies of the processing pathway in mammalian cells both *in vitro* and *in vivo* [57,66,103]. An appropriate PCR fragment designed to contain a T7 promoter sequence linked to the *pre-mir-30* sequence was generated and used for *in vitro* transcription of a 71 nt *pre-mir-30* RNA. To prepare a substrate for *in vitro* processing, the RNA was uniformly labeled with [α-^{32}P]UTP. Processing of labeled *pre-mir-30* was examined by incubation for 90 min with protein extracts prepared from primary neurons and astrocytes (see Section B.2.6.2 for details). As controls, mock processing reactions were performed in which the reaction was stopped immediately after addition of cell extract by heating the reaction (80 °C) in the presence of denaturing 2× RNA Loading Dye Solution. Reaction products were examined by denaturing gel electrophoresis and subsequent autoradiography. Incubation with either cell extract led to the release of a single novel band compared to the mock incubation (0 min, lanes 1 and 2), or to precursor RNA migration without any cell extracts (90 min, lane 5). The processing product is indicated with an arrow in Figure C.13 A. This processing product co-migrated with a synthetic 22nt RNA run in parallel, and visualized by ethidium bromide staining (not shown). Formation of the processing product was markedly higher after incubation of pre-*mir-30* with neuronal extract than with astrocyte extract. (Figure C.13 A, lanes 4 and 3 respectively).

Next, the *in vitro* processing assay was performed with cell extracts from undifferentiated or differentiated ES and EC cells (Figure C.13 B and C). Processing activity of ES cell-derived neuronal precursors (N) was enhanced compared to undifferentiated ES cells (U) or ES cells induced to form cardiomyocytes (C) (Figure C.13 B, compare lanes 2, 3 and 4). Neural induction also led to increased processing activity using P19 EC cells (Figure C.13 C, compare lanes 1 and 2).

To confirm that the observed product is *bona fide mir-30* mature miRNA a trace amount of purified recombinant Dicer RNAse was added to a processing reaction containing neuronal extracts from EC cells. As expected, addition of Dicer led to enhanced accumulation of the processing product (Figure C.13 lane 3).

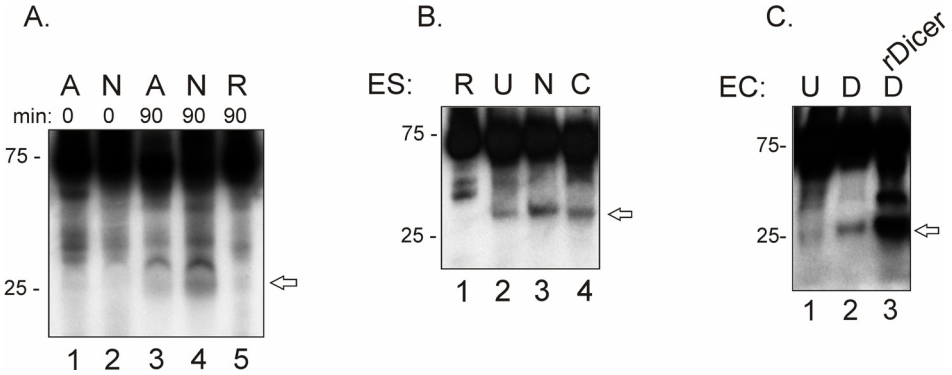

Figure C.13. *In vitro* processing of the *mir-30* precursor. **Panel A:** Cytoplasmic extracts from E17 embryonic neurons (N) or astrocytes (A) were incubated either in a mock reaction for 0 min (**Lanes 1 and 2**) or for 90 min (**Lanes 3 and 4**) with radioactive labeled ~71 nt *mir-30* precursor RNA. **Lane 5** is the RNA substrate incubated without addition of extract. The position of ~22 nt mature *mir-30* is marked with an arrow to the right, migration of markers run in parallel are given to the left. **Panel B:** Processing reactions contained either no extract (R, **Lane 1**), extracts from undifferentiated ES cells (U, **Lane 2**); ES cell-derived neural progenitors (N, L**ane 3**); or ES cell-derived cardiomyocytes (C, **Lane 4**). **Panel C:** processing reactions were incubated with extracts from undifferentiated EC cells (U, **Lane 1**); or EC cells 8 days after neural differentiation (D, **Lanes 2 and 3**); in **Lane 3** 0.25 units purified recombinant Dicer protein were incubated with pre-*mir30*.

These experiments established the *in vitro* assay as a useful tool for the investigation of miRNA processing activity across developmental cell types. Given the evidence for differential regulation of *let-7* processing in neuronal cell types, these experiments were repeated using an appropriate construct for the generation of pre-*let-7a*. For comparison, an additional construct for generation of the highly expressed and neuron specific pre-*mir-128* was also tested. These substrate RNAs were designed to contain a 2 nt overhang in order to more accurately correspond to available models for Drosha cleavage. This modification of the substrates appeared to result in improved cleavage in the *in vitro* assay. Incubation of radioactively labeled pre-*let-7a* with cytoplasmic extracts from differentiated EC cells led to the release of a novel band compared to input RNA (Figure C.14 A, lanes 1-4). This product represents the 22 nt *let-7* form as evidenced by two criteria: it co-migrated with a synthetic 22 nt oligoribonucleotide run in parallel and visualized by ethidium bromide staining (not shown), and with the product obtained after digestion of pre-*let-7a* RNA with recombinant Dicer protein (lane 5). *let-7a* processing activity was very low in extracts from undifferentiated EC cells (lane 2) and was strongly increased 12 days after induction of neural differentiation by RA treatment (lane 4). Similar results were obtained with pre-*let-7e* (data not shown).

To determine if the increase in processing activity was specific for pre-*let-7*, the experiment was repeated with the neuron-specific *mir-128* precursor as substrate (Figure C.14 B). *mir-128*

processing activity also showed a clear correlation with the differentiation state of the cells. Incubation of pre-*mir-128* with extracts from Day 8 or 12 cells (lanes 3 and 4), but not undifferentiated cell extract (lane 2), led to release of a 22 nt RNA that co-migrated with the digestion product formed after incubation with recombinant Dicer (lane 1).

Therefore, in primary cells, as well as the ES and EC cell models, those cell types that accumulate the highest levels of mature miRNAs display the highest levels of *in vitro* pre-miRNA processing activity.

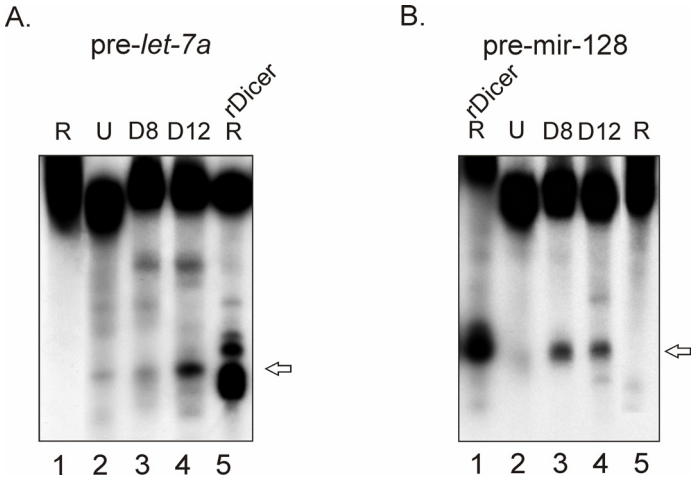

Figure C.14. *In vitro* miRNA processing by differentiated P19 EC cells. **Panel A:** Pre-*let-7a* was incubated in a processing reaction in the absence of added protein extract (R, **Lane 1**), with extracts prepared from undifferentiated EC cells (U, **Lane 2**), RA-stimulated EC cells cultured for 8 days (D8, **Lane 3**) or 12 days (D12, **Lane 4**), or digested with purified recombinant Dicer protein (R, rDicer, **Lane 5**). Reaction products were analyzed by denaturing gel electrophoresis. The position of ~22 nt *let-7a* is indicated by an arrow. **Panel B:** Pre-*mir-128* RNA was employed in the processing assay as described for Panel A. Digestion products obtained after incubation with recombinant Dicer (R, rDicer, **Lane 1**), extract from undifferentiated EC cells (U, **Lane 2**), RA-stimulated EC cells cultured for 8 days (D8, **Lane 3**) or 12 days (D12, **Lane 4**), and without adding protein (R, **Lane 5**). The position of ~22 nt *mir-128* is indicated by an arrow.

In addition to the difference in the level of processing activity, significantly higher pre-*let-7* and pre-*mir-30* binding activity was also observed in neuronal extracts or extracts from differentiated EC cells, as evidenced by the formation of a slowly migrating complex after electrophoresis of the native processing reaction (Figure C.15). Formation of the complex appeared to correlate with processing activity of the various extracts, suggesting that the complex might reflect pre-miRNA specific protein binding. In the case of EC cells, the apparent pre-*let-7* binding activity increased during the course of neural differentiation (Figure C.15 A, lanes 1-4). Similarly, strong complex assembly was observed with neuronal but not astrocytic extracts (Figure C.15 A, compare lanes 6 and 7). Complex assembly was not restricted to pre-*let-7*, as similar results were obtained using pre-*mir-30* (Figure C.15 A, compare lanes 9 and 10). The complex was eliminated by phenol/chloroform extraction of the reaction products, indicating that covalent RNA-RNA or RNA-protein bonds are not involved (data not shown). As a test for the functional significance of the observed complexes, the effect of ATP on binding activity was examined. Although miRNA

cleavage by purified mammalian Dicer is ATP-independent, ATP is believed to increase subsequent resolution of the reaction products [151,152]. Addition of ATP to the processing reaction strongly reduced the level of bound complex (Figure C.15 A, compare lanes 9 and 11). As a control, complex formation was not observed on an RNA fragment transcribed from the GFP gene (Figure C.15 A lanes 13-15). As further evidence for a functional relevance of the protein-RNA complex, the effect of FMRP antibody on precursor binding activity was tested. Addition of a monoclonal FMRP antibody, but not a control antibody specific for the astrocyte marker S100β, led to a partial supershift of the protein/RNA complex, indicating the presence of the mRNP component FMRP (Figure C.15 B).

It should be noted that these experiments were conducted in parallel to the processing assay and were obtained using a denaturing gel system. Although urea is frequently used to suppress non-specific binding in protein-RNA interaction studies, it was nevertheless surprising to observe robust RNA binding in the denaturing gel system used in these experiments. These experiments therefore served as the starting point for the investigation of precursor-binding by non-denaturing electrophoretic mobility shift assay (EMSA) after establishment of optimal conditions ([49], and data not shown). These experiments confirmed and extended the results presented here, demonstrating that processing activity correlated with a neuron-enhanced binding complex shown by antibody challenge to contain the miRISC proteins Ago1 and FMRP.

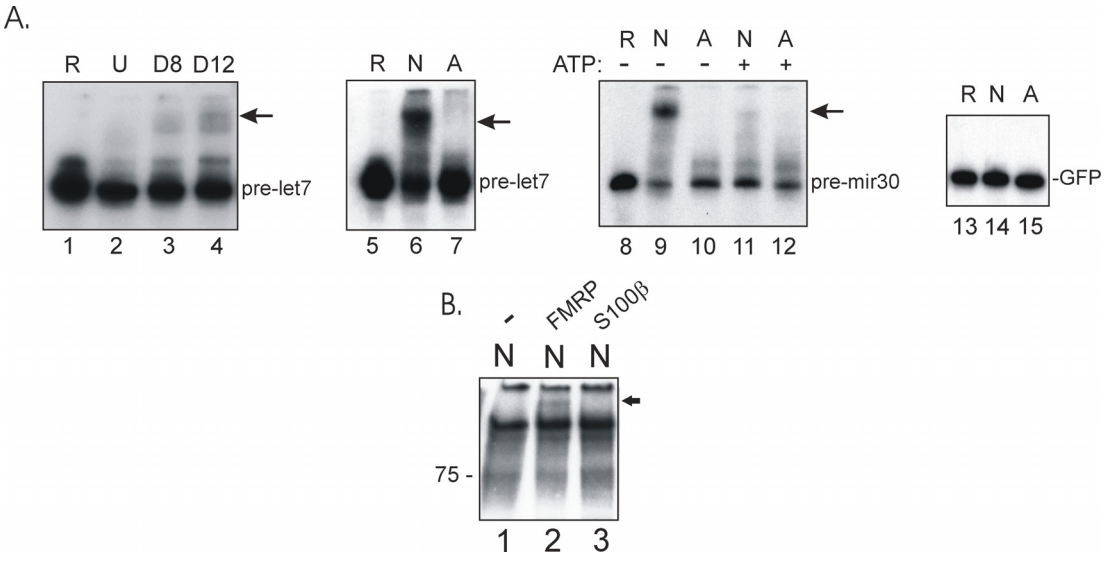

Figure C.15. Analysis of miRNA precursor binding complexes during *in vitro* processing reaction. **Panel A:** Binding complexes formed during *in vitro* processing reactions were visualized after denaturing gel electrophoresis. The identity of the substrate RNA is indicated to the right. **Lane 1** is input RNA without extract (**R**). **Lanes 2-4** show the results obtained with EC cell extracts. **Lane 2** is undifferentiated extract (**U**), **Lane 3** is differentiated cells isolated on Day 8 (**D8**) and **Lane 4** differentiated cells isolated on Day 12 (**D12**). Complex formation with differentiated cell extracts is marked by an arrow. **Lanes 5-15** present complexes formed with primary neuron (**N**) and astrocyte (**A**) extracts as indicated above each lane. In **Lanes 8-12** the effect of ATP addition or omission on complex formation is tested as indicated. **Lanes 13 to 15** demonstrate lack of binding to a control RNA derived from the eGFP coding region. **Panel B** displays binding complexes formed after incubation of labeled pre-*mir-30* with extracts from primary neurons (**N**). Migration of probe with neuronal extract is shown in **Lane 1**. Neuronal extracts were preincubated with anti-FMRP antibody (**Lane 2**) or control anti-S100β antibody (**Lane 3**). Complex formation with FMRP antibody is marked by an arrow. Supershift complex is sensitive to anti-FMRP antibody (**Lane 2**) but not control antibody (**Lane 3**).

C.3.2. Expression analysis of miRISC components

With the exception of germ cells, which possess a distinct complement of miRISC proteins, the miRNA pathway was previously thought to be ubiquitous. However, the possibility of developmental regulation had not been directly addressed. The expression of all known components of the miRISC was examined by RT-PCR. In Figure C.16, it was confirmed that mRNA levels for most of the known components of the miRISC (Dicer, Ago1, Gemin3, Gemin4, MOV10, TNRC6B, and TRBP2) were similar in neurons, compared to astrocytes, and did not significantly change in the course of ES or EC cell differentiation. However, in the case of FMRP an approximately two to three fold elevation was observed in the mRNA level after neural induction of ES cells, whether by RA treatment or by monolayer induction. No increase was observed in ES cell-derived cardiomyocytes. Surprisingly, FMRP mRNA levels were reproducibly similar in neurons and astrocytes, and RA treatment of EC cells also did not detectably induce FMRP message.

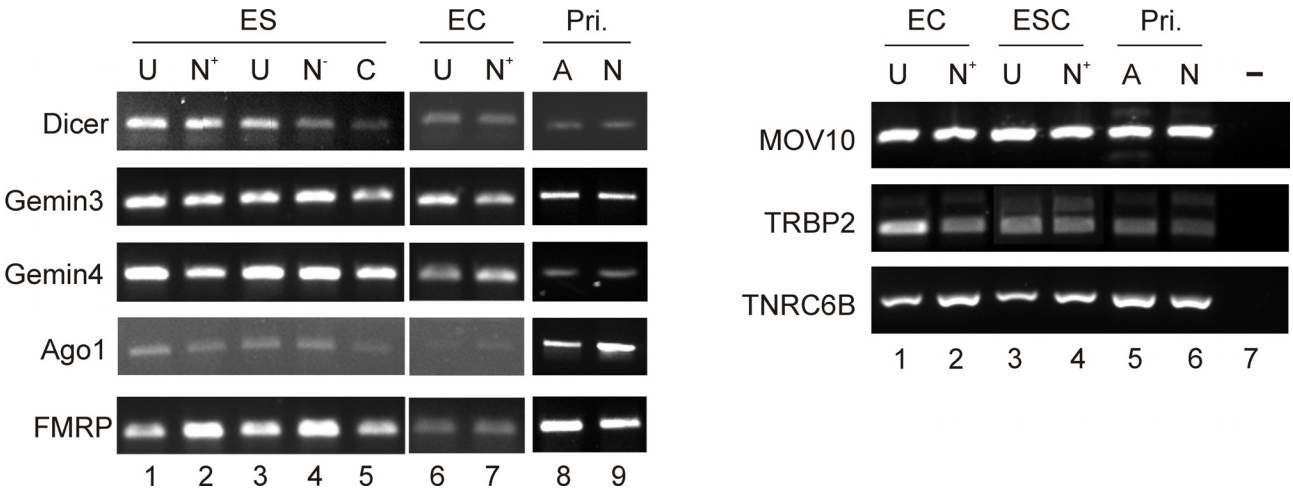

Figure C.16. Semi-quantitative RT-PCR analysis of miRISC components. cDNA samples were prepared from ES, EC cells, and primary (**Pri.**) embryonic astrocytes (**A**) and neurons (**N**). ES samples were taken from undifferentiated cells (**U**); cells stimulated with RA and cultured for 24 days ($\mathbf{N^+}$); cells undergoing neural differentiation in defined medium ($\mathbf{N^-}$); or ES cell-derived cardiomyocytes (**C**). EC samples were from undifferentiated cells (**U**) or cells stimulated with RA and cultured for 8 days ($\mathbf{N^+}$). Genes targeted by primer pairs are given on the left. Note the increased signal for FMRP (Lanes 2 and 4). "-" is negative PCR control without any template.

Therefore, FMRP expression was examined at the protein level. In Western blots, FMRP protein levels were elevated in primary neurons in comparison with primary astrocytes (Figure C.17 A) Immunofluorescence experiments revealed FMRP protein co-localizing with the neuron–specific marker MAP2 in P19 EC-derived neurons (Figure C.17 B). Finally, higher levels of FMRP association with pre-miRNAs were observed by EMSA in extracts from embryonic neurons compared with astrocytes [49].

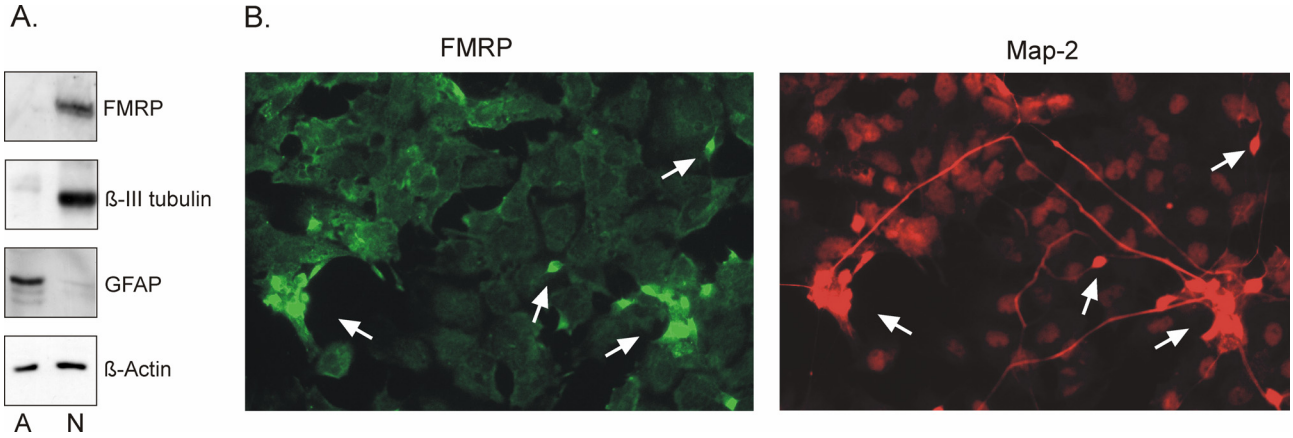

Figure C.17. FMRP expression in primary neurons and neural differentiated P19 EC cells**. Panel A**: Western blot analysis of cytoplasmic extracts from astrocytes (**A**) and neurons (**N**), as indicated below each lane, was probed with antibodies against FMRP (clone 1C3), neuron specific β-III Tubulin, astrocytes specific GFAP and β-actin. **Panel B**: Immunocytochemistry of neural differentiated EC cells revealing high-level FMRP expression (green) in MAP2 positive cells (red). Arrows designate double-positive cells.

These results are compatible with previous reports describing neuron-specific FMRP expression and the role of post-trancriptional mechanisms in FMRP regulation [153,154]. Taken together, these results are consistent with the presence of the core miRISC components in all cell types examined. However, neuron-enhanced expression of the accessory miRISC component FMRP correlated with increased processing activity and precursor RNA binding activity found in neuronal cell types. The function of FMRP in the miRNA pathway is currently under investigation, it will be interesting to determine if it is directly involved in miRNA processing by the miRISC.

C.3.3. Cellular localization of miRISC components

C.3.3.1. Localization of miRISC components in HEK293 cells

During the course of this work, a number of studies were published showing that in human cells Ago1 and Ago2 proteins are not randomly distributed, but concentrate in mRNA decay centers called cytoplasmic bodies or P-bodies [92,95-97]. Moreover, it was observed that miRNAs and their target mRNAs are also localized to P-bodies [96,97]. Given the evidence for differential activity of the miRNA pathway during stem cell differentiation, it was interesting to examine localization of the pathway as a function of differentiation state. As a first step, it was necessary to establish a cellular assay system. For this reason, constructs expressing Flag/HA-tagged human Argonaute proteins Ago1 and Ago2, which are fully functional for siRNA-mediated silencing, were obtained from the laboratory of Thomas Tuschl. HEK293 cells were transfected with these constructs, and the subcellular localization was determined. In agreement with previously published reports, Flag/HA-Ago1 and Flag/HA-Ago2 were observed in discrete, brightly staining cytoplasmic foci, although some Ago1 and Ago2 may also be distributed throughout the cytoplasm (Figure C.18 A).

Both the size of individual foci and the number of foci varied between individual cells with an average of three to ten clear foci per cell. Endogenous Ago1and Ago2 could also be detected in discrete foci with an average number of two to three foci per cell (Figure C.18 B). Differences in foci numbers are probably due to overall weaker signals from anti-Ago1 or anti-Ago2 polyclonal antibodies in comparison with monoclonals that recognize epitope-tagged proteins. Alternatively, ectopic overexpression of the proteins may lead to the formation of additional P-bodies.

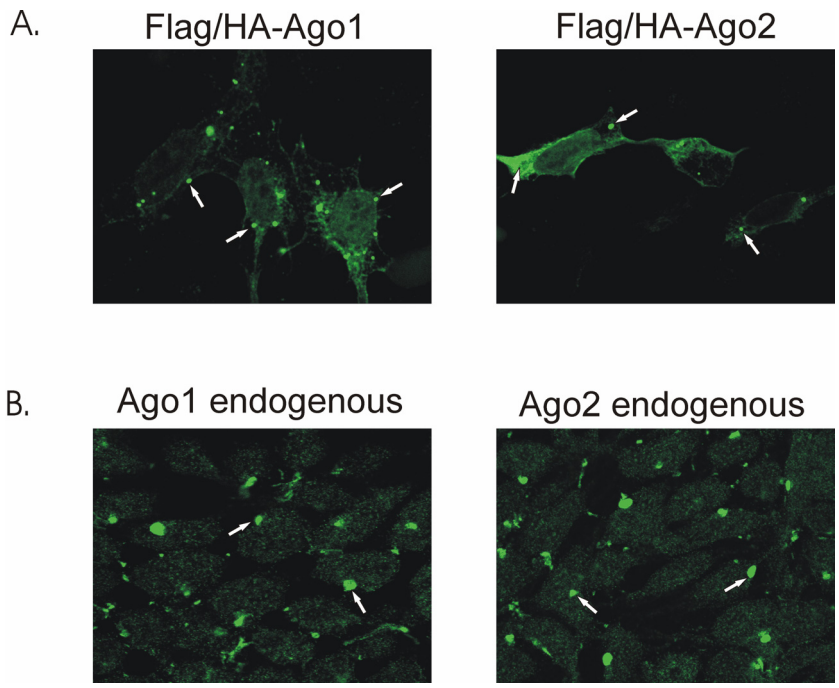

Figure C.18. Ago1 and Ago2 proteins are localized in HEK293 cells to discrete cytoplasmic foci. **Panel A** demonstrates the HEK293 cells transfected either with Flag/HA-Ago1 or Flag/HA-Ago2 constructs. Cells were visualized using anti-Flag monoclonal antibody (mAb) that recognizes the Flag epitope contained on Ago1 or Ago2. The localizations of endogenous Argonaute proteins are shown in **Panel B**. In this case cells were stained with anti-Ago1 and anti-Ago2 polyclonal antibodies respectively.

To further confirm these results, Ago1 and Ago2 were shown to co-localize with the GW182 protein as well as two other components of the miRISC, MOV10 and TNRC6B to P-bodies. GW182 is involved in mRNA metabolism and is a well-established marker for P-bodies [94]; TNRC6B is a protein homolog of GW182. Flag/HA-Ago1 and Flag/HA-Ago2 were transiently co-transfected either with Myc-tagged MOV10 or Myc-tagged TNRC6B constructs and stained with mouse anti-Flag and rabbit anti-Myc antibodies respectively. Endogenous GW182 protein was detected with anti-GW182 polyclonal antibody (Figure C.19). In all experiments, Ago1 and Ago2 consistently displayed similar localization patterns, representative results for Ago2 are presented in Figure C.19.

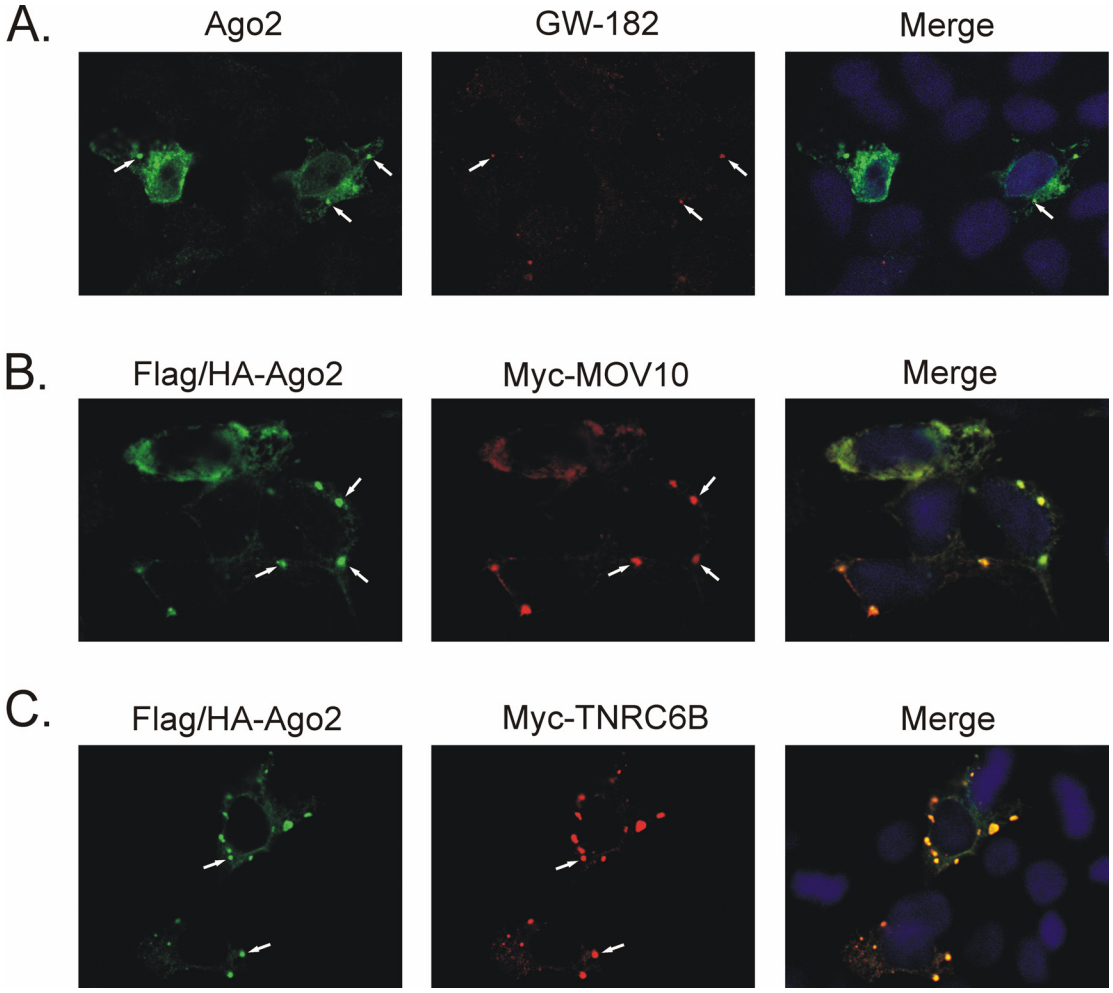

Figure C.19. Co-localization of Ago2 with GW182, MOV10 and TNRC6B to P-bodies. **Panel A**: HEK293 cells were transfected with Flag/HA-Ago2. After 24 hours cells were fixed and stained with rabbit anti-Ago2 polyclonal antibody (green) and mouse anti-GW182 mAb (red). **Panel B**: HEK293 cells were co-transfected with Flag/HA-Ago2 and Myc-MOV10 constructs. After 24 hours cells were stained with mouse anti-Flag mAb (green) and rabbit anti-Myc polyclonal antibody (red). **Panel C**: Co-transfection of HEK293 cells with Flag/HA-Ago2 and Myc-TNRC6B. Ago2 protein was visualized using anti-Flag antibody (green), TNRC6B was visualized using anti-Myc antibody (red). Localization of Ago1 protein had the similar localization patterns and is not shown.

Given the known association of FMRP with the miRISC, Flag-tagged FMRP was co-transfected with Ago1, Ago2, MOV10 or TNRC6B constructs. The results are shown in Figure C.20. Both Argonaute proteins and TNRC6B displayed partial overlap with FMRP in distribution and co-localization to P-bodies (Panels A, B and C). However, in the case of co-transfection with MOV10 co-localization of FMRP to P-bodies was not observed. FMRP was uniformly distributed throughout the cytoplasm while MOV10 was localized to P-bodies (Figure C.20 D). These results point to differences in the interaction of FMRP with individual components of the miRISC. Failure of MOV10 to attract FMRP to P-bodies suggest the lack of a direct interaction between the two proteins, as has been demonstrated for Argonaute proteins and MOV10 [92]. Nevertheless, the ability of Ago1, Ago2 and TNRC6B to influence FMRP localization is consistent with the known association of FMRP with the miRISC and suggests that FMRP may play a functional role in P-bodies.

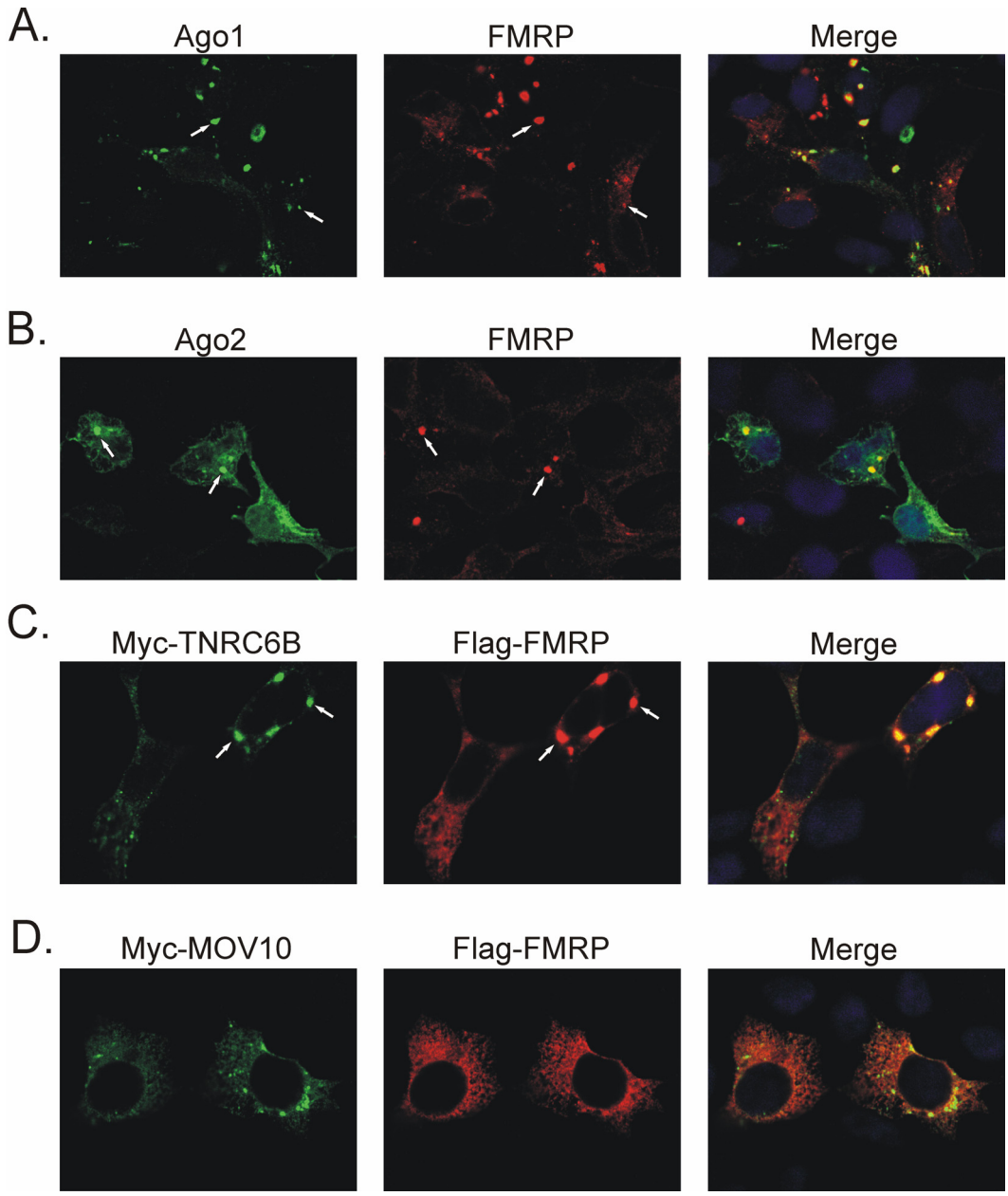

Figure C.20. FMRP expression in HEK293 cells and co-localization with other components of miRISC. Cells were transfected with Flag-FMRP construct and either with Flag/HA-Ago1, Flag/HA-Ago2, (**Panels A** and **B**), Myc-TNRC6B (**Panel C**) or Myc-Mov10 (**Panel D**). Note the absence of P-bodies by FMRP staining in **Panel D**. In **Panels A** and **B**, cells were stained with rabbit anti-Ago1 or anti-Ago2 polyclonal antibodies respectively (green) and with mouse anti-FMRP mAb (red). In **Panels C** and **D** cells were visualized using rabbit anti-Myc polyclonal antibody (green) and mouse anti-Flag mAb (red).

C.3.3.2. Localization of miRISC components in EC and ES cells

Subsequently, the subcellular localization of Ago1, Ago2 and FMRP was investigated in ES and EC cells. In contrast to HEK293 cells, in approximately 90% of transfected ES/EC cells diffuse cytoplasmic staining was observed for each of the three proteins after transfection, without discernible concentration to defined subcellular structures. These results were obtained using the anti-Flag antibody, an FMRP constructs as well as polyclonal sera specific for each of proteins

tested. Representative plates for Ago1 in ES, and Ago1, Ago2 and FMRP in EC cells, are presented in Figure C.21.

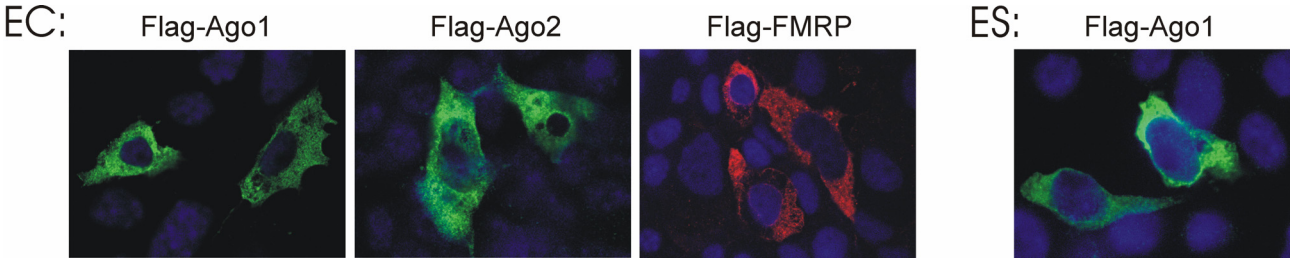

Figure C.21. Localization of miRNA processing proteins in stem cells. Flag-tagged Ago1, Ago2 and FMRP proteins were expressed in EC and in ES cells, as indicated above each plate. Cells were stained with anti-Flag mAb. Argonaute proteins and FMRP both displayed diffuse cytoplasmic staining.

To determine if ES or EC cells lack P-bodies, localization of ectopically expressed MOV10 and TNRC6B, two integral components of P-bodies[92], was assayed. Both localized to cytoplasmic foci in EC cells (data not shown), suggesting that despite the diffuse distribution of the Argonaute proteins, EC cells do contain P-bodies. Since it has been shown that Argonaute proteins physically interact with MOV10 and TNRC6B, co-transfection experiments were performed to determine if MOV10 or TNRC6B exert an influence on Argonaute, and also FMRP, localization. Under these conditions, both MOV10 and TNRC6B were able to re-localize Ago1 or Ago2 to P-bodies. Representative results for Ago1 are shown in Figure C.22 A and B and suggest that the signals governing localization of Argonaute in stem cells may be overridden or saturated by ectopic expression of MOV10 or TNRC6B.

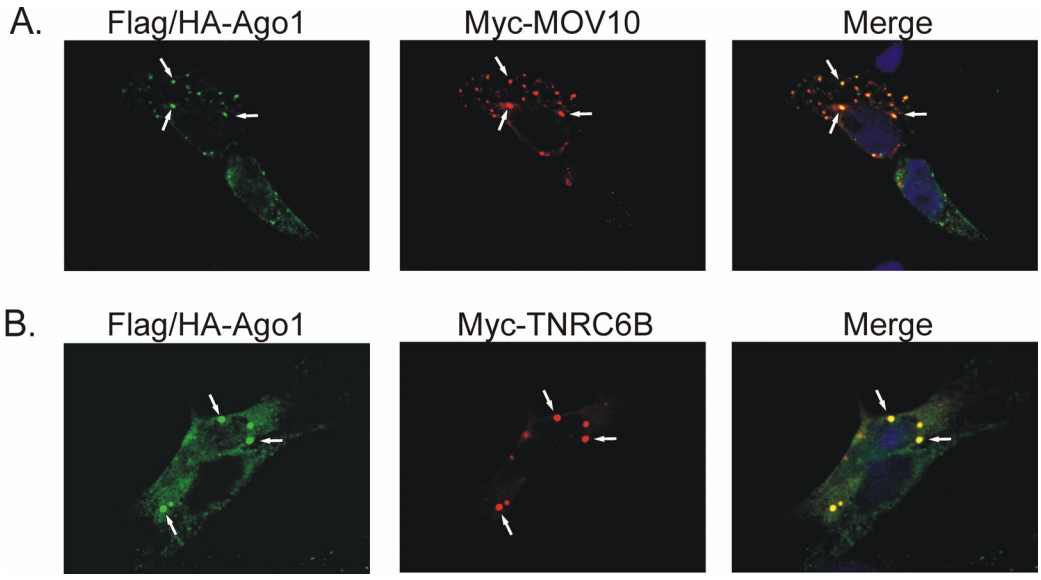

Figure C.22. Re-localization of Ago1 to P-bodies. **Panel A:** cells were co-transfected with expression vectors for Flag-tagged Ago1 and Myc-tagged MOV10. Ago1 was visualized with anti-Flag mAb (green), MOV10 with rabbit anti-Myc (red). Representative foci marked by arrows. **Panel B:** EC cells were co-transfected with expression vectors for Flag-tagged Ago1 and Myc-tagged TNRC6B, as described in panel A. Note dependence of Ago1 localization on TNRC6B expression comparing the two cells shown. TNRC6B negative cell shows cytoplasmic localization of Ago1 protein, while TNRC6B positive cell contains Ago1 in P-bodies.

In the same assay, the integral P-body protein TNRC6B was able to partially attract FMRP to cytoplasmic foci (Figure C.23 A). The effect was specific, as the Ago1 interacting protein MOV10 had no obvious effect on FMRP distribution in stem cells (Figure C.23 B).

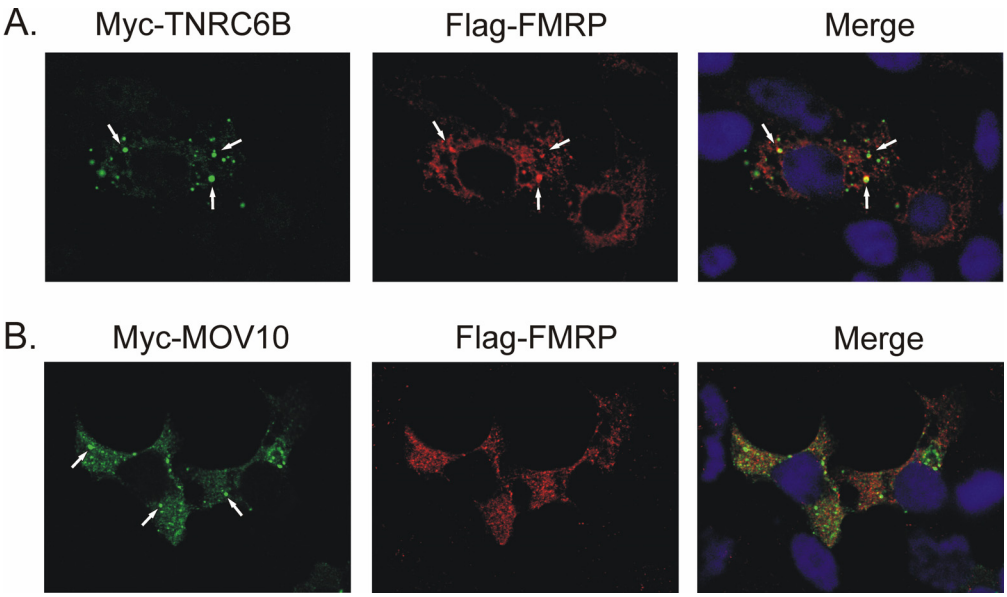

Figure C.23. Localization of FMRP, MOV10 and TNRC6B in P19 EC cells. **Panel A:** EC cells were co-transfected with expression vectors for Flag-tagged FMRP and Myc-tagged TNRC6B, and stained as described in Figure C.22. Partial re-localization of FMRP to TNRC6B-tagged foci was observed, examples are marked by arrows. **Panel B:** EC cells were co-transfected with expression vectors for Flag-tagged FMRP and Myc-tagged MOV10. MOV10 was unable to pull down FMRP to P-bodies.

C.3.3.3. Localization of miRISC components in primary hippocampal neurons

The results presented in Section C.3.3.2 suggest that regulatory interactions may control miRISC organization during differentiation. Given the evidence implicating FMRP and MOV10 in miRNA-mediated neuronal translation [141,142,155], the subcellular localization of miRISC protein components was examined in cultured hippocampal neurons by transfection. Transfected Ago1, Ago2, FMRP and MOV10 displayed a characteristic punctate distribution in the dendritic arbors. In contrast, distribution in the soma was diffuse. Co-localization of Ago1 with MOV10, and FMRP with MOV10 to dendritic foci is shown in Figure C.24 A and B. To better visualize the MOV10 localization in relation to dendritic structures such as branch points and spines, MOV10 and eGFP were co-transfected (Figure C.24 C). The two proteins did not co-localize, and MOV10 staining can be seen to frequently underlie dendritic spines. A different pattern was obtained with TNRC6B, which was primarily found in bright foci in the soma and proximal dendrites (Figure C.24 D). TNRC6B was able to attract Ago1 to the same foci in the soma. If these results accurately reflect the localization of the endogenous proteins, it will be interesting to functionally characterize the discrete compartments occupied by MOV10 and TNRC6B in mature neurons.

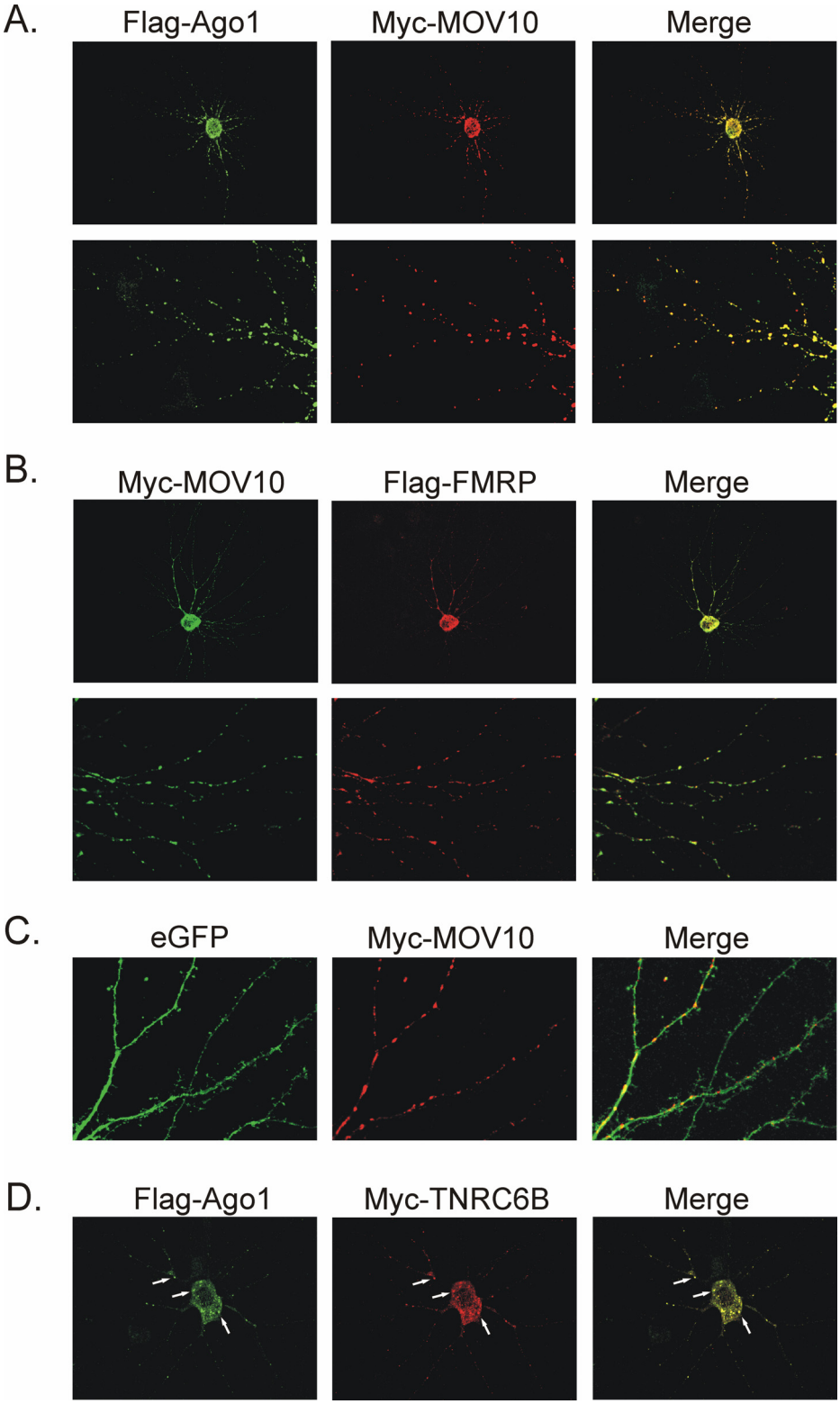

Figure C.24. Localization of miRNA processing proteins in cultured hippocampal neurons. **Panel A: N**eurons were co-transfected with expression vectors for Flag-tagget Ago1 and Myc-tagged MOV10. Ago1 was visualized with mouse anti-Flag mAb (green), MOV10 - with rabbit anti-Myc (red). The top panels provide an overview of a positive neuron, the lower panels a detailed view of dendritic staining. **Panel B:** Neurons were co-transfected with expression vectors for Flag-tagged FMRP and Myc-tagged MOV10. FMRP was visualized with anti-Flag mAb M2 (red), MOV10 with rabbit anti-Myc (green). An overview and detailed view of dendritic staining are provided as above. **Panel C:** Detailed view of dendritic staining of a neuron co-transfected with expression vector for eGFP and Myc tagged MOV10. Cells were stained for GFP (anti-GFP mAb, green) and MOV10 (rabbit anti-Myc, red). **Panel D:** Flag-tagged Ago1 and Myc-tagged TNRC6B were co-transfected and visualized with anti-Flag mAb (green), and anti-Myc (red), respectively. Staining was confined to foci in the neuronal soma and proximal dendritic arbor, three examples are marked with arrows.

C.4. Functional analysis of miRNAs

C.4.1. Establishment of experimental system

In order to assay for miRNA functional activity, reporter gene assays were developed that were suitable for use in primary and ES/EC cell cultures. For this reason, well-characterized miRNA binding sites from *C. elegans* target genes (*lin-41* for *let-7* and *lin-4* for *mir-125*) have been used, as well as synthetic targets containing multiple artificial binding sites for *mir-128*. Target sites were inserted into the 3'UTR of the eGFP gene mRNA encoded on the reporter plasmid peGFP-N1 (see Materials and methods, Section B.2.5.6 and Scheme B.1 and Scheme B.2 for details). The principle of the cloning strategy is presented in Figure C.25.

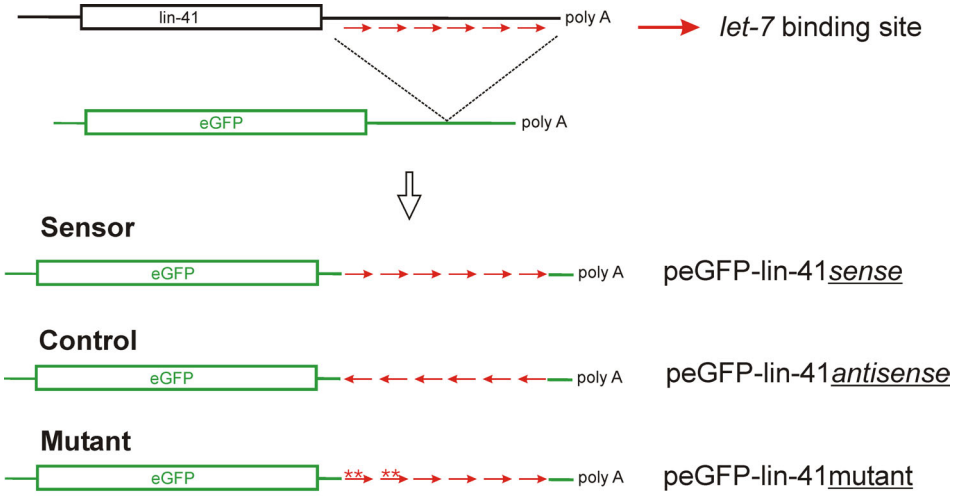

Figure C.25. Cloning strategy on the example of *let-7* sensor construct. A ~500 bp fragment was amplified from the 3'UTR region of *lin-41* gene. *let*-7 is predicted to bind to six sites in the 3' UTR of its target gene, *lin-41*, to down-regulate LIN-41 translation. Then the DNA fragment, containing all *let-7* binding sites was cloned into peGFP-N1 vector in 3'UTR region of *eGFP* mRNA in sense and antisense orientation yielding the sensor plasmid (peGFP-lin-41 S) and antisense control (peGFP-lin41 AS). As the second control, 4 point mutations were introduced into *let-7* complementary sites 1 and 2 (marked with asterisks). *mir-125* sensor plasmid and antisense control were designed by the same strategy. *lin-4* (*C. elegans* homolog for *mir-125* is predicted to bind to seven sites in the 3'UTR of the *lin-14* gene, to down-regulate LIN-14 translation).

The target sites were cloned in sense and antisense orientations, yielding sensor plasmids (S) and the antisense control plasmids (AS). In the case of *lin-41*, a third plasmid was generated carrying point mutations in the *let-7* binding sites. Vella and colleagues have shown that two of the conserved *let-7* complementary sites (designated LCS1 and LCS2) are necessary and sufficient for down-regulation of *lin-41* [25]. Furthermore, the nucleotides 2-7 at the 5' end of a miRNA (the "seed" region) are most critical for target recognition [110,156]. Therefore, in the negative control mutant two nucleotides were exchanged in the 3' region of both LCS1 and LCS2 (Scheme C.1).

Scheme C.1. Disruption of the *let-7* complementary sites in *lin-41* sensor plasmid by point mutations. Mutations are marked with a grey colour.

These constructs and the parent vector peGFP-N1 were introduced into undifferentiated P19 EC cells yielding similar transfection efficiencies and average fluorescent intensities. Stable transfectants were generated by selection with geneticin, allowing sensor expression to be monitored over a two-week course of *in vitro* neural differentiation with RA. eGFP expression was quantified by flow cytometry, or analyzed at the single cell level by fluorescence microscopy. Primary E15 or E17 astrocyte cultures were transfected in duplicate with the sensor and control constructs, and eGFP expression was quantified by flow cytometry relative to the peGFP-N1 vector. Relative activity of the sensor constructs was also examined after electroporation of E15 neuronal cultures.

C.4.2. Neuron-specific suppression of *let-7* and *mir-125* sensor plasmids

let-7, *mir-125* and *mir-128* are highly represented in the expression libraries from adult brain tissue. Neuronal specificity in their expression (Northern blots, Figure C.4) suggested that these miRNAs may play a role in differential mRNA utilization between neurons and astrocytes. Because primary cultures are not entirely free of contaminating cell types, it was important to verify neuron-specific expression at the cellular level and test whether neuron-specific expression is reflected functionally.

C.4.2.1. Visualization of let-7, mir-125 and mir-128 in cortical neurons

Relative activity of the sensor constructs in primary neurons was examined either after transfection with Fugene6 reagent or after electroporation of E15 neuronal cultures. The two methods complement each other, in that Fugene6 transfection yields a relatively low efficiency but with good preservation of neuronal morphology and in electroporation morphology is compromised but efficiencies as high as 40% are obtained. Neuronal identity of the overwhelming majority of transfected cells was confirmed by co-staining with neuron-specific β-III Tubulin antibody (see Materials and Methods, Figure B.1 B).

First, for *let-7*, *mir-125* and *mir-128* sensor assays, neuronal cultures were transfected in duplicate after 4 to 7 days in culture using Fugene6. After 48 hours cells were stained with an anti-GFP antibody and anti-β-III Tubulin antibodies. Double-positive cells were tallied manually, double-blind by inspection using immunofluorescence microscopy (Figure C.26, Figure C.27).

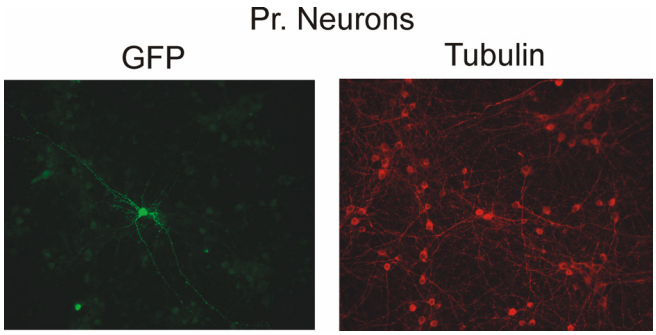

Figure C.26. Primary neurons were transfected with peGFP-lin-14 AS construct. After 48 hours cells were stained with anti-GFP polyclonal antibody and with anti-β-III Tubulin mAb. Double positive cells were counted.

eGFP expression was efficiently suppressed for all three sensor constructs compared to control (Figure C.27 A, B and C, n=3, p<0.01). For *let-7,* the average reduction in three independent experiments was 9-fold, for *mir-125* a 20-fold and for *mir-128* a 4-fold reductions were observed.

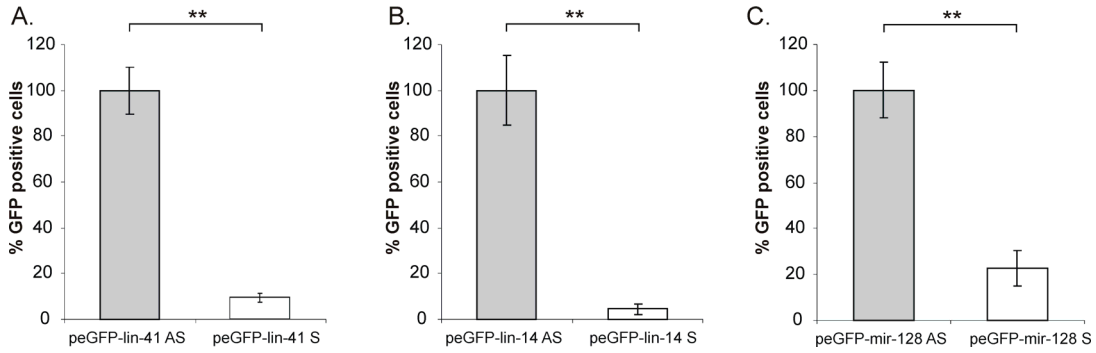

Figure C.27. A, B and C. eGFP$^+$/Tubulin$^+$ cells were quantified after lipofection of primary cortical neurons. Average cell count/transfection is compared for control plasmids (grey bars) and sensor plasmids (white bars), standard error of the mean (SEM) is indicated. Nine-fold reduction was observed for *let-7* sensor, 20-fold for *mir-125* sensor and 4-fold for *mir-128* sensor. Statistical significance for the decrease of eGFP expression in sensor transfectants was confirmed using the *t*-test (n=3, p<0.01)

In addition, transfection efficiencies sufficient for quantification by flow cytometry have been achieved using electroporation of E15 cortical neurons. For these experiments *let-7* and *mir-125* sensors have been chosen, as E15 is too early for high-level *mir-128* expression.

After electroporation of primary neurons with *let-7* constructs, quantification of eGFP-expressing cells by flow cytometry revealed very similar levels for the antisense and point mutant compared to the parent peGFP-N1 vector. The *let-7* sensor, however, was strongly downregulated. eGFP-expressing cells were reduced to 20% of the control (Figure C.28 A, n=6, p<0.0001). Average fluorescence intensity was more strongly affected than the tally of eGFP-positive cells, as is apparent from the corresponding flow cytometry plots (Figure C.28 B).

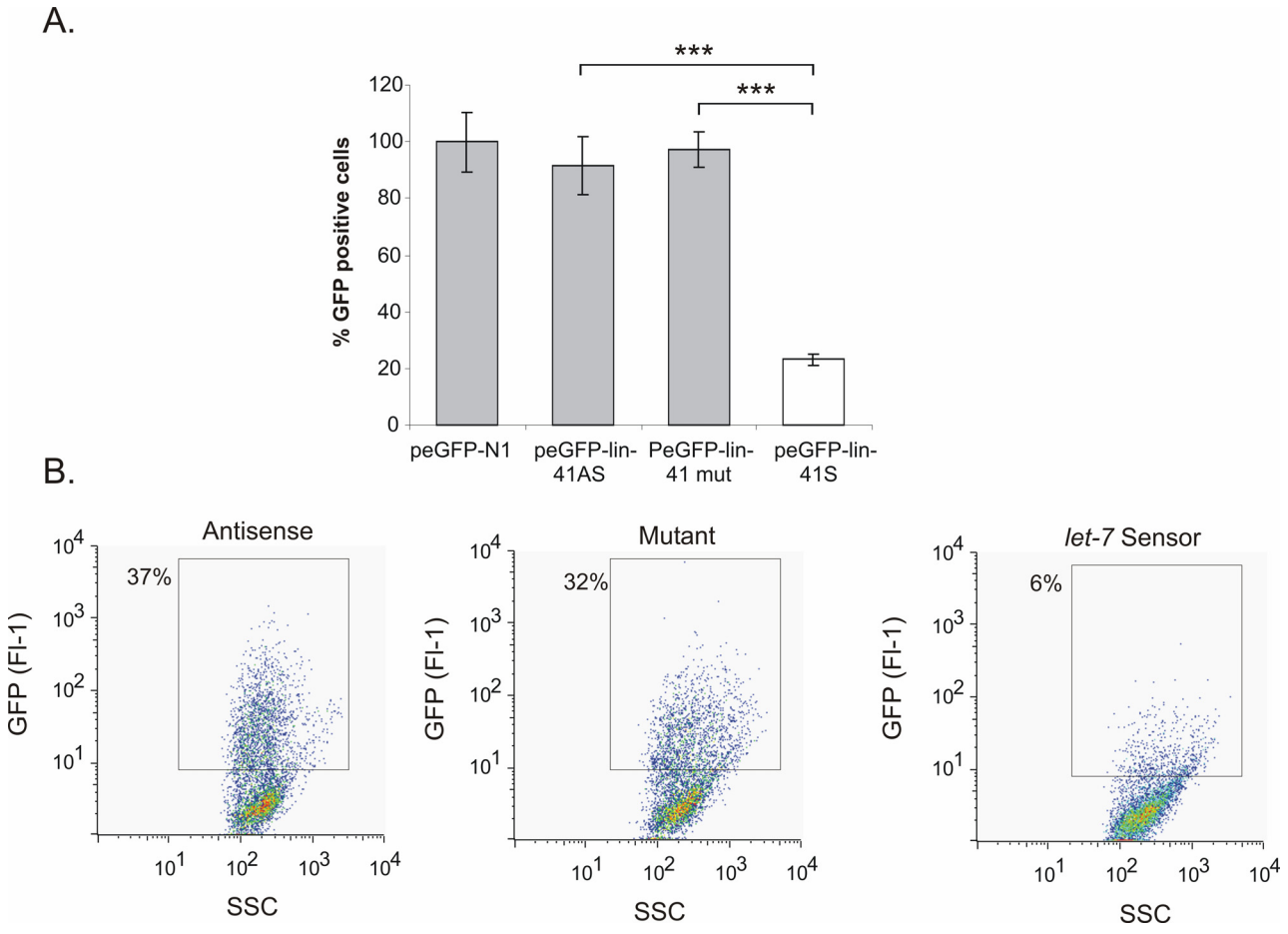

Figure C.28. *let-7* sensor expression after transfection in embryonic neurons. **Panel A:** eGFP expression was quantified by flow cytometry 72 hours after electroporation and is shown for each plasmid tested relative to the parent vector peGFP-N1. Grey bars give results for the control plasmids and white bar for the sensor plasmid**.** For each column SEM is indicated; statistical significance for the eGFP reduction in sensor expression was confirmed using the *t*-test (n=6, p<0.0001). **Panel B:** Representative flow cytometry plots of eGFP expression (GFP Fl-1) versus side scatter (SSC). Gates were established with untransfected cells, for each population the percentage of positive-gated cells is given.

In the case of the *mir-125* sensor, neuronal eGFP expression was readily apparent in cells transfected with the control construct, and was strongly reduced in sensor transfectants (Figure

C.29 A and B). Average reduction in eGFP^{+} cells was 27-fold (n=4, p<0.001, Student's paired t-test). Representative dot plots from one experiment are presented in Figure C.29 C.

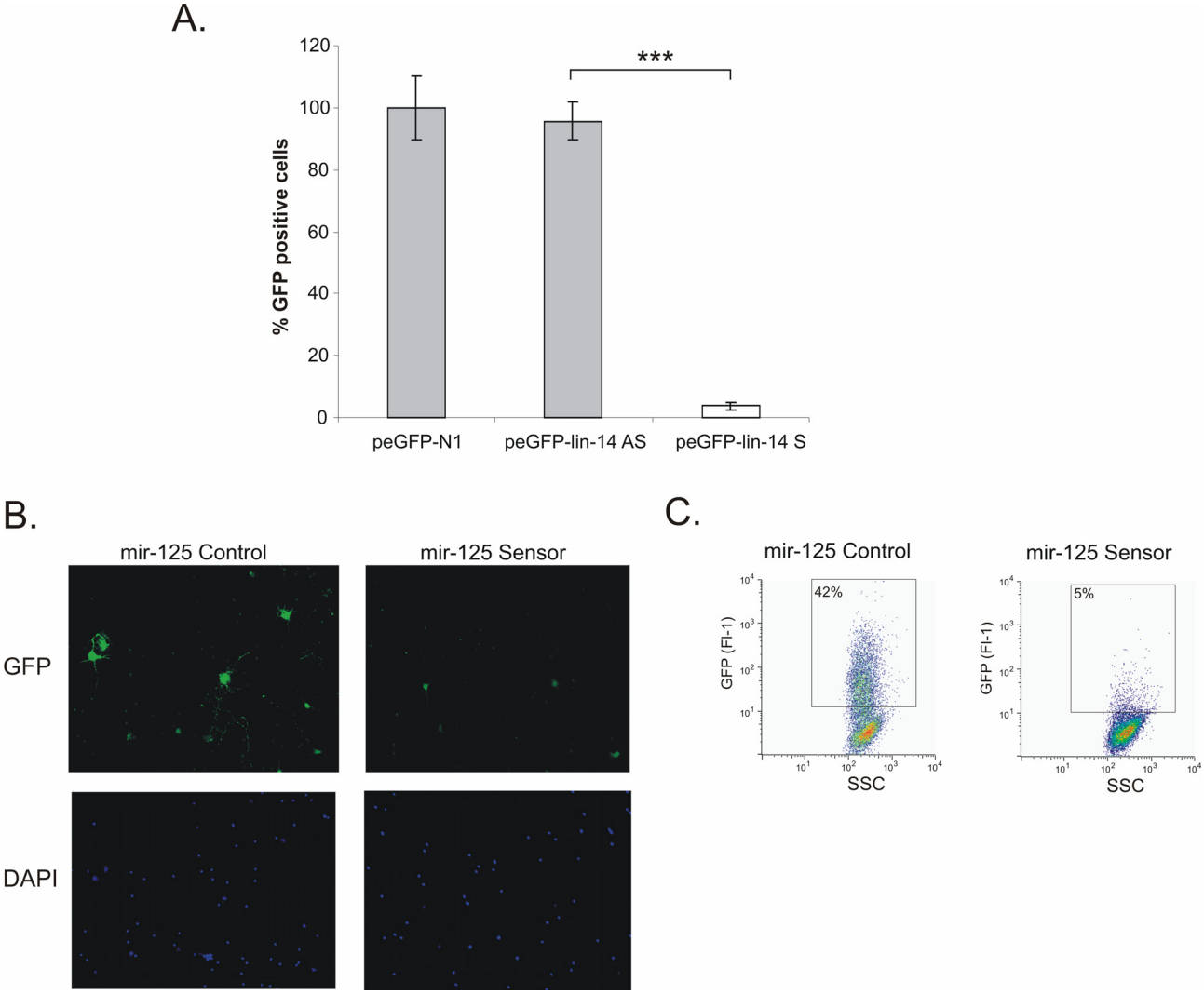

Figure C.29. Regulation of the *mir-125* sensor transcript in primary neurons. **Panel A:** eGFP expression was quantified by flow cytometry in 72 hours after transfection and expressed for each plasmid tested relative to the parent vector peGFP-N1. Grey bars give results for the control plasmids and white bar for the sensor plasmid**.** For each column SEM is indicated; statistical significance for the eGFP reduction in sensor expression was confirmed using the t-test (n=4, p<0.001).**Panel B:** eGFP expression was visualized by fluorescence microscopy (20×) after transfection with the *mir-125* sensor or control plasmid, as indicated. Representative fields are shown, together with corresponding nuclear staining. **Panel C:** Representative flow cytometry plots of eGFP expression (GFP Fl-1) versus side scatter (SSC). Gates were established with untransfected cells, for each population the percentage of positive-gated cells is given.

These experiments confirm the efficient suppression of the *let-7* and *mir-125* sensors in neuronal cells.

C.4.2.2. Visualization of let-7, mir-125 and mir-128 in primary astrocytes

In the next round of experiments, primary astrocyte cultures were prepared in parallel to the neuron cultures and transfected with the *let-7*, *mir-125* and *mir-128* sensor constructs. Cell purity of cultured astrocytes was confirmed by staining with an antibody against the astrocyte marker GFAP

(75% of GFAP positive cells; see Materials and Methods, Figure B.1 A). In the case of *let-7*, in four independent experiments the proportion of eGFP-expressing cells was essentially equivalent for peGFP-N1, the antisense and the mutant control plasmids. In contrast, eGFP expression mediated by the *let-7* sensor plasmid was modestly suppressed (43% of control, n=4, p<0.01), but not as strong as in neurons, consistent with low levels of *let-7* activity in astrocytes (Figure C.30 A). Representative flow cytometry plots are presented in Figure C.30 B.

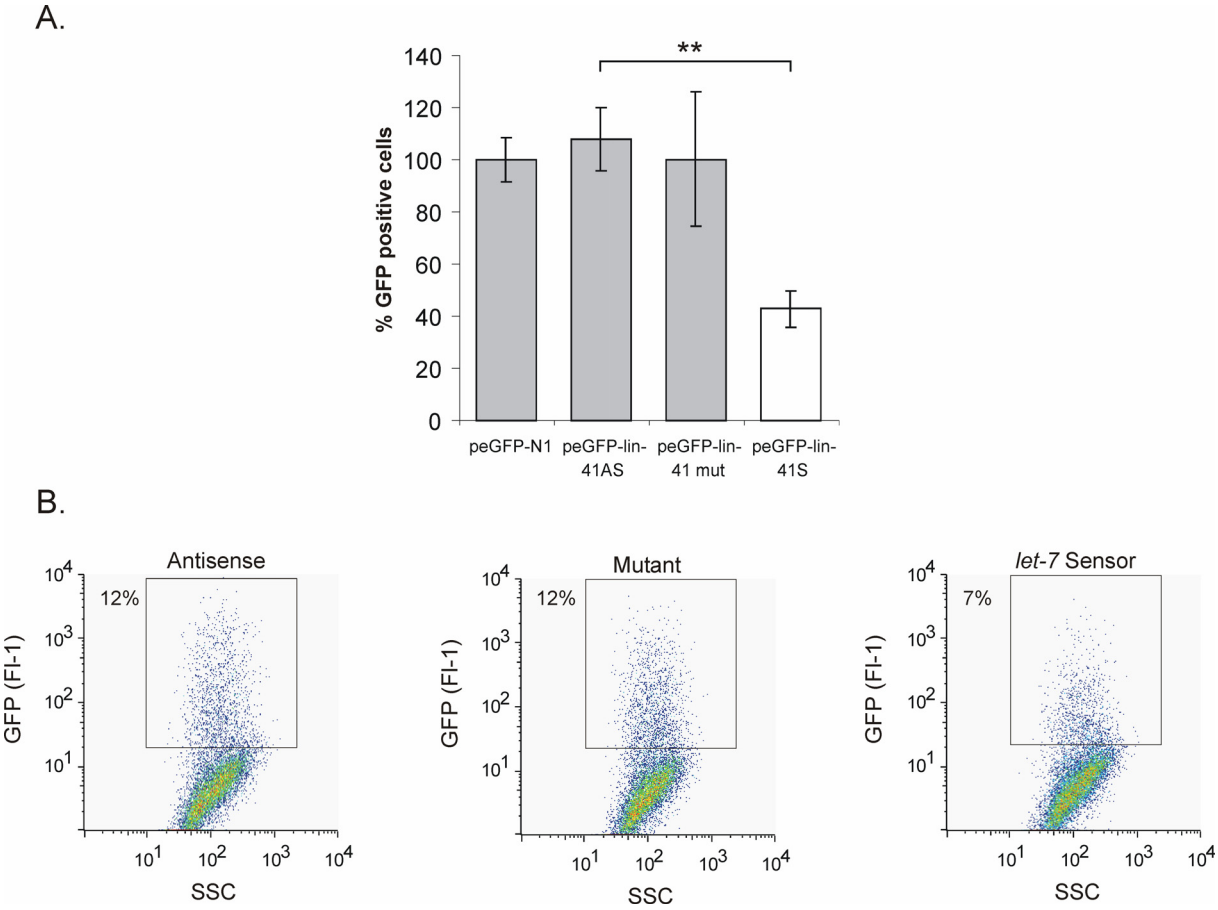

Figure C.30. *let-7* sensor expression in embryonic astrocytes. **Panel A:** eGFP expression was quantified by flow cytometry 48 hours after transfection and expressed for each plasmid tested relative to the parent vector peGFP-N1. Grey bars give results for the control plasmids and white bar for sensor plasmid**.** For each column (SEM) is indicated; statistical significance for the eGFP reduction in sensor expression was confirmed using the Student's paired *t*-test (n=4, p<0.01). Differences in eGFP expression between sensor and mutant plasmid were not significant. **Panel B:** Representative flow cytometry plots of eGFP expression (GFP Fl-1) versus side scatter (SSC). Gates were established with untransfected cells, for each population the percentage of positive-gated cells is given.

In the case of *mir-125*, the presence of *mir-125* binding sites in the sensor plasmid led to a 2- to 3-fold reduction in eGFP-positive cells compared to the antisense control, as quantified by flow cytometry (n=4, p<0.0001, Student's paired *t*-test) (Figure C.31 A, B).

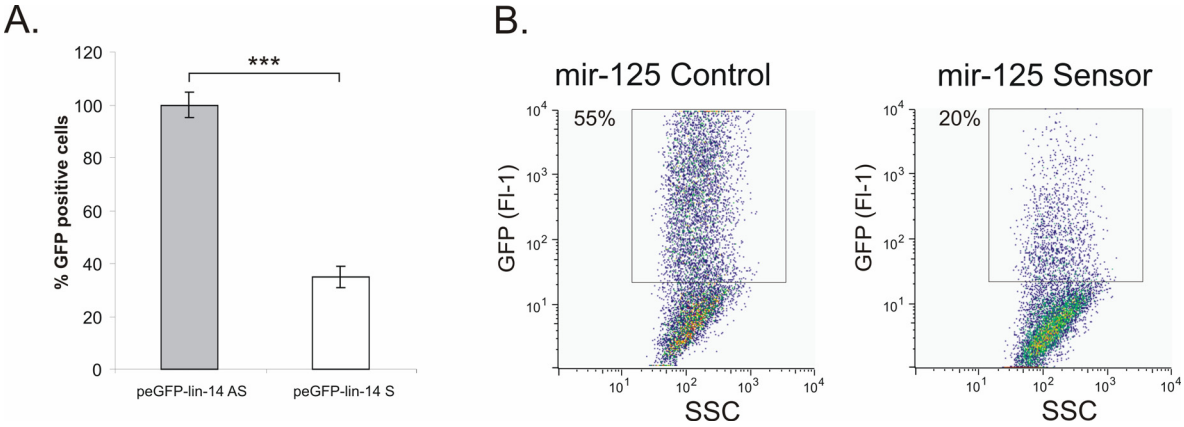

Figure C.31. Regulation of the *mir-125* sensor transcript in primary astrocytes. eGFP expression was quantified by flow cytometry 48 hours after transfection. **Panel A**: eGFP expression in control was taken as 100%. White bar gives results for sensor plasmid and grey bar for the antisense control plasmid. For each column SEM is indicated. Statistical significance for the eGFP reduction in sensor expression was confirmed using the *t*-test (n=4, p<0.0001). **Panel B:** Representative flow cytometry plots of eGFP expression (GFP Fl-1) versus side scatter (SSC). Gates were established with untransfected cells, for each population the percentage of positive-gated cells is given.

In the case of the *mir-128* sensor, no statistically significant difference in eGFP expression was observed compared to control (Figure C.32 A, B, n=4).

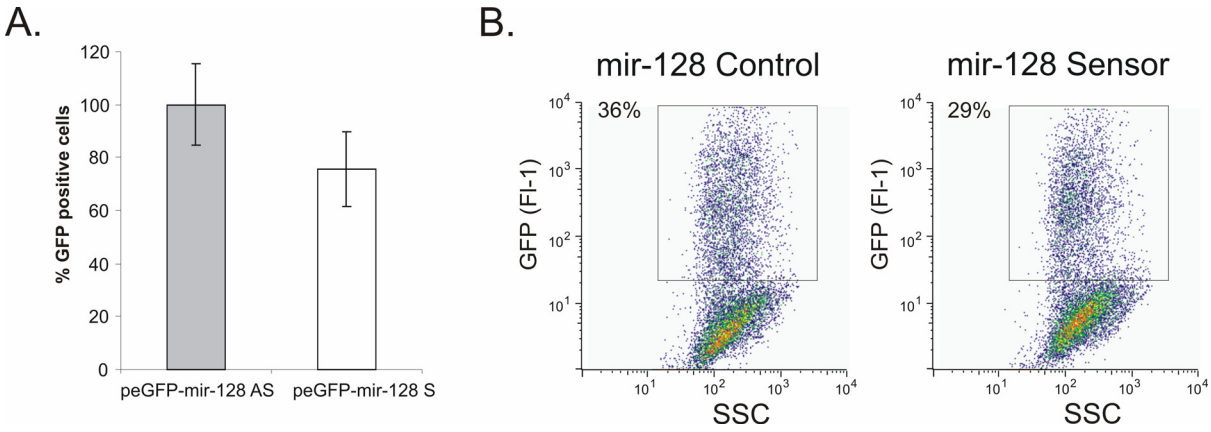

Figure C.32. *mir128* sensor expression after transfection in primary astrocytes. eGFP expression was quantified by flow cytometry 48 hours after transfection. **Panel A**: eGFP expression in control was taken as 100%. White bar gives results for sensor plasmid and grey bar for the antisense control plasmid. For each column SEM is indicated. **Panel B:** Representative flow cytometry plots of eGFP expression (GFP Fl-1) versus side scatter (SSC). Gates were established with untransfected cells, for each population the percentage of positive-gated cells is given.

Representative plates of cells transfected in parallel and processed for immunocytochemistry are shown in Figure C.33 A and B, and support the conclusion that *mir-128* is inactive and *mir-125* weakly active in cultured astrocytes.

The experiments with primary cell cultures confirm the efficient suppression of the *let-7* and *mir-125* sensors in neuronal cells.

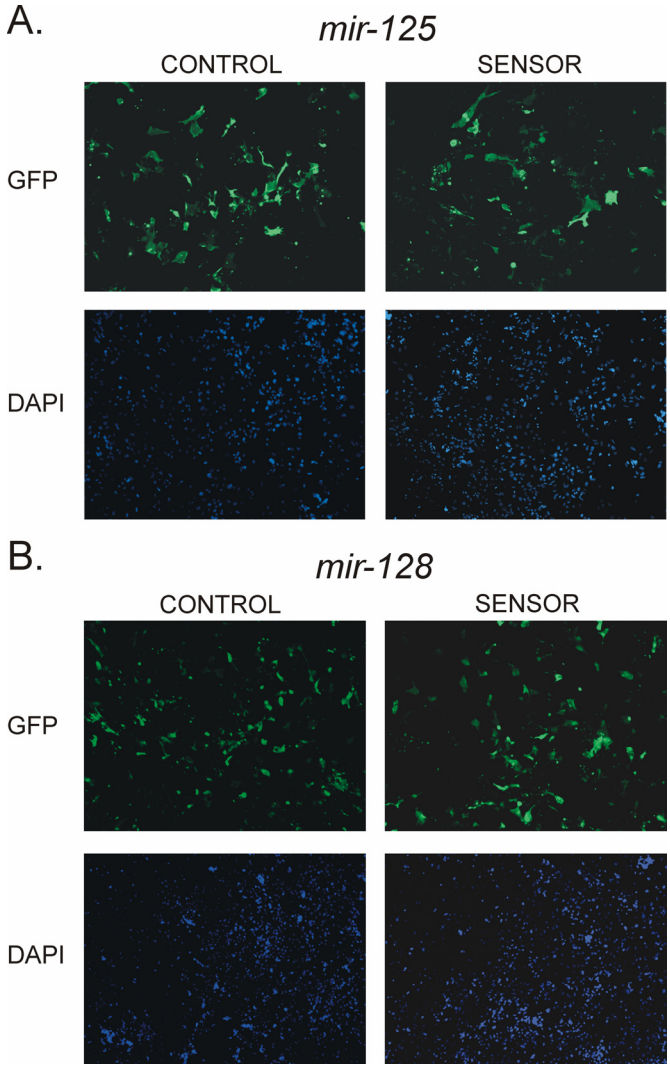

Figure C.33 A and B. eGFP expression was visualized by fluorescence microscopy (10×) after transfection with the *mir-125* and *mir-128* constructs. Representative fields for control and sensor plasmids are shown, together with corresponding DAPI nuclear staining.

C.4.2.3. Downregulation of let-7 and mir-125 sensors in EC cells after induction of neural differentiation

To study regulation of the sensor during neural differentiation, pooled, stable transfectants of peGFP-lin-41 S, peGFP-lin-14 S and control AS or mutant plasmids were generated in EC cells. Transfected P19 EC cells were first selected with G418 for two weeks and then eGFP-positive cells were collected by two rounds of fluorescence assisted cell sorting. For all constructs, the cultures were routinely tested for eGFP expression by flow cytometry. The transfection efficiency was about 60-80%. Next, neural differentiation of the stable transfectants was induced (see Materials and Methods, Section B.2.1.1 for details) and the cells were assayed by immunocytochemistry and flow cytometry. Representative plates of cell populations transfected either with the *let-7* sensor or control plasmids are presented in, demonstrating a profound reduction of GFP fluorescence in cells containing the sensor plasmid after stimulation of neural differentiation. Neuronal identity of the

transfected cells was confirmed by counterstaining with a neuron-specific anti-β-III Tubulin antibody (Figure C.34, red).

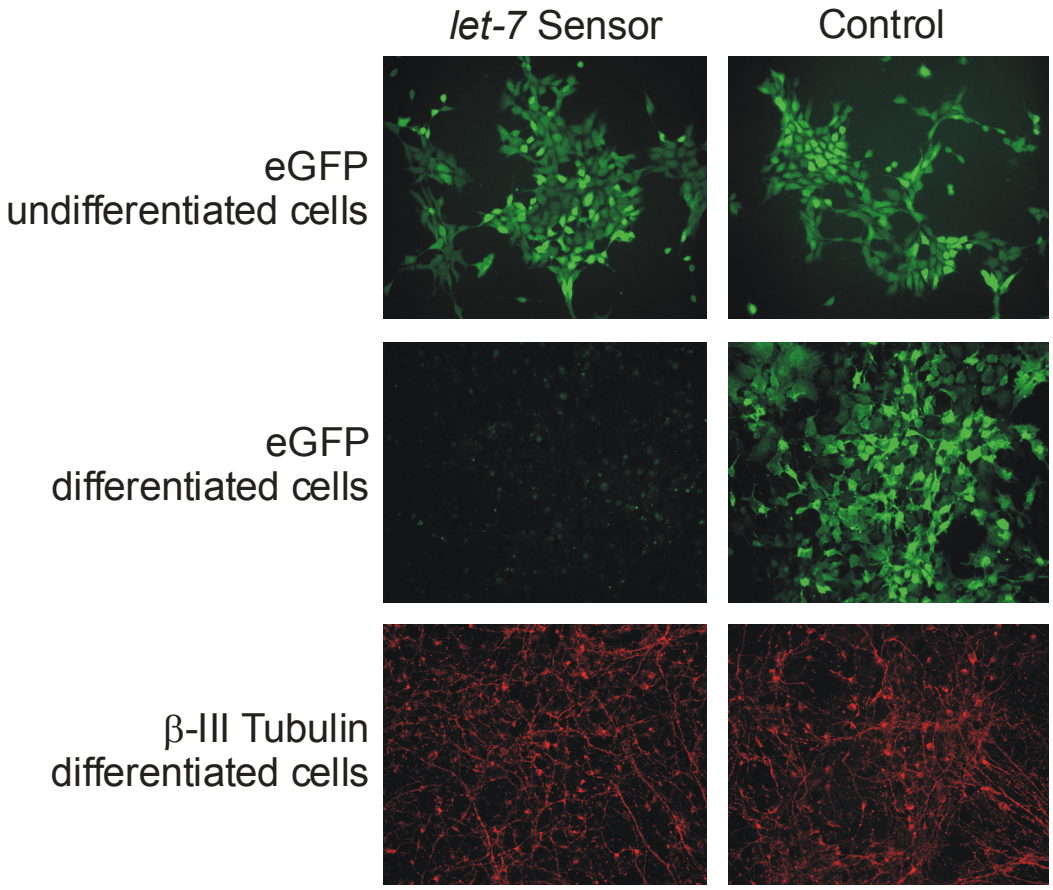

Figure C.34. Efficient downregulation of the *let-7* sensor in EC-derived neurons. The plates represent the sensor and control transfectants prior to (U, EC cells) and 12 days after stimulation with RA (D, EC cells). For differentiated cultures, neuronal phenotype is demonstrated by staining with the anti-β-III Tubulin antibody.

To verify if the downregulation of *let-7* sensor is neuron-specific further immunostaining of differentiated P19 EC cells was performed. Stable transfectants were induced with RA and stained with neuron (NeuN, MAP2 or β–III Tubulin) and astrocyte (GFAP, S100β) specific markers 12 days after neural induction. Neuron specific downregulation of the *let-7* sensor in differentiated EC cells was observed. β-III Tubulin positive cells did not express eGFP, while GFAP and S100β positive cells remained green (Figure C.35). NeuN and MAP2 positive cells were also eGFP-negative (data not shown).

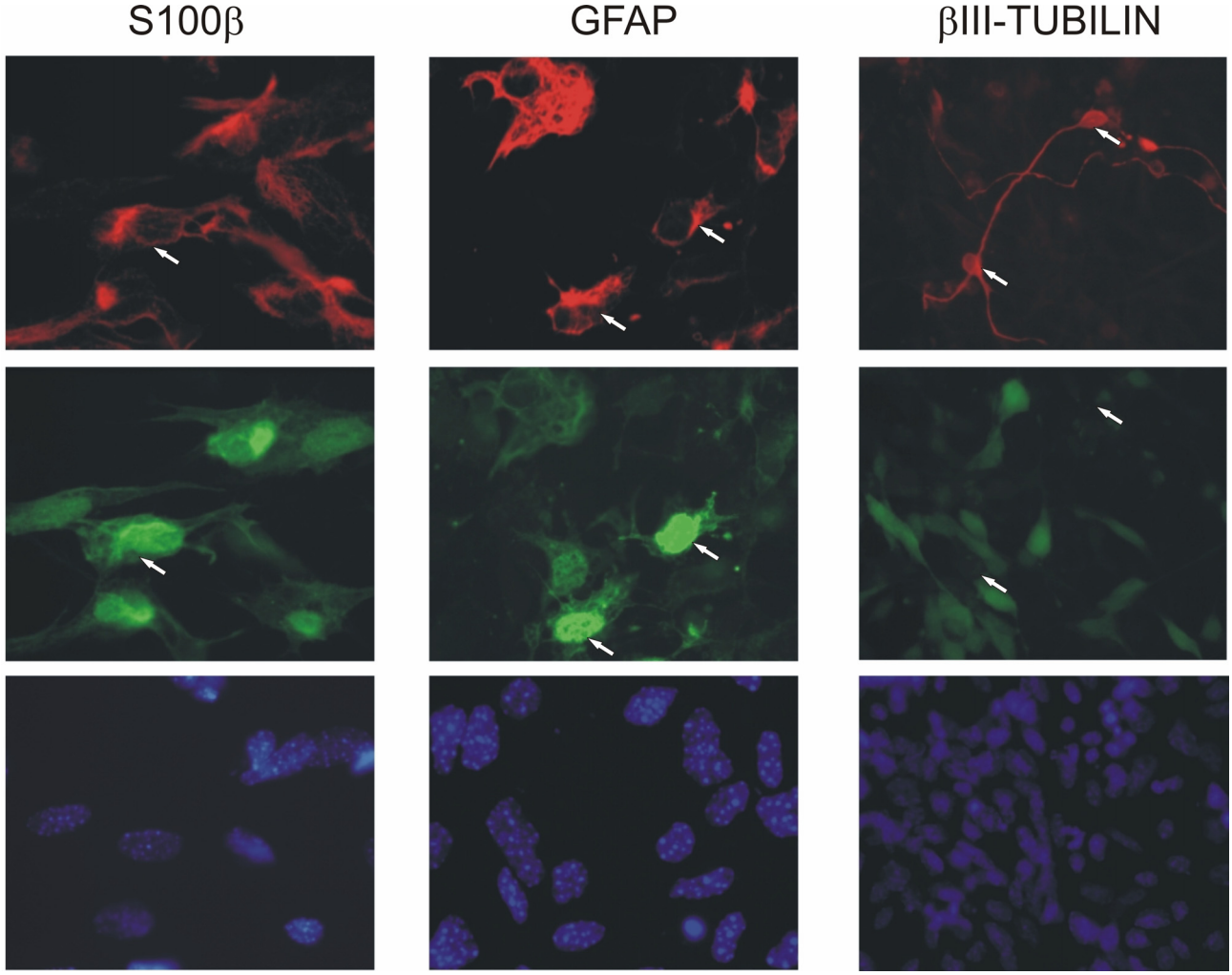

Figure C.35. Neuron-specific downregulation of *let-7* sensor expression in differentiated P19 EC cells. Stable transfected EC cells were neural induced with RA and cultivated on coverslips. Cells were fixed and stained on Day 12 after RA stimulation. eGFP expression of sensor transfectants is shown in the middle panel. Results of indirect immunofluorescence with anti-GFAP, anti-S100β or anti-β-III Tubulin antibodies (red) and nuclear staining with Hoechst dye (blue) are shown. Notice the downregulation of eGFP expression in β-III Tubulin-positive cells.

In order to quantify the results obtained by immunocytochemistry eGFP expression was determined by flow cytometry. Six independent flow cytometry assays are summarized in Figure C.36, and representative flow cytometry plots are shown in Figure C.37 A and B. eGFP expression in undifferentiated EC cells was set at 100%. As expected, in cells containing the control constructs the relative proportion of eGFP-positive cells did not appreciably change when assayed 12 days after RA treatment, compared to untreated (undifferentiated) cells. In comparison, RA treatment of cells containing the *let-7* sensor construct decreased the number of eGFP-positive cells to 35%.

An even greater reduction of eGFP expression after neural differentiation was observed in the peGFP-lin-14 S transfected cells (Figure C.38, Figure C.39 A and B). A twenty-fold reduction of eGFP expression was observed in the cells containing *mir-125* sensor plasmid after neural differentiation ($n=6$, $p<0.001$).

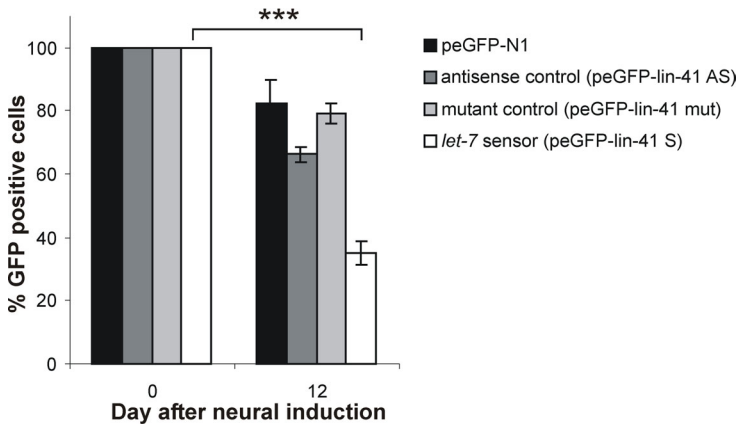

Figure C.36. Quantitative analysis of eGFP expression in EC cells stably transfected with a *let-7* sensor (white bar, peGFP-lin-41S); the antisense control plasmid (dark grey bar, peGFP-lin-41AS); the mutant control plasmid (light grey bar, peGFP-lin-41 mut); or the parent plasmid peGFP-N1 (black bar) as indicated to the right. The proportion of $eGFP^+$ cells determined by flow cytometry prior to neural induction was set at 100% and compared to $eGFP^+$ cells 12 days after neural induction with RA. Data are from six independent experiments (n=6, $p<0.001$, Student's paired *t*-test).

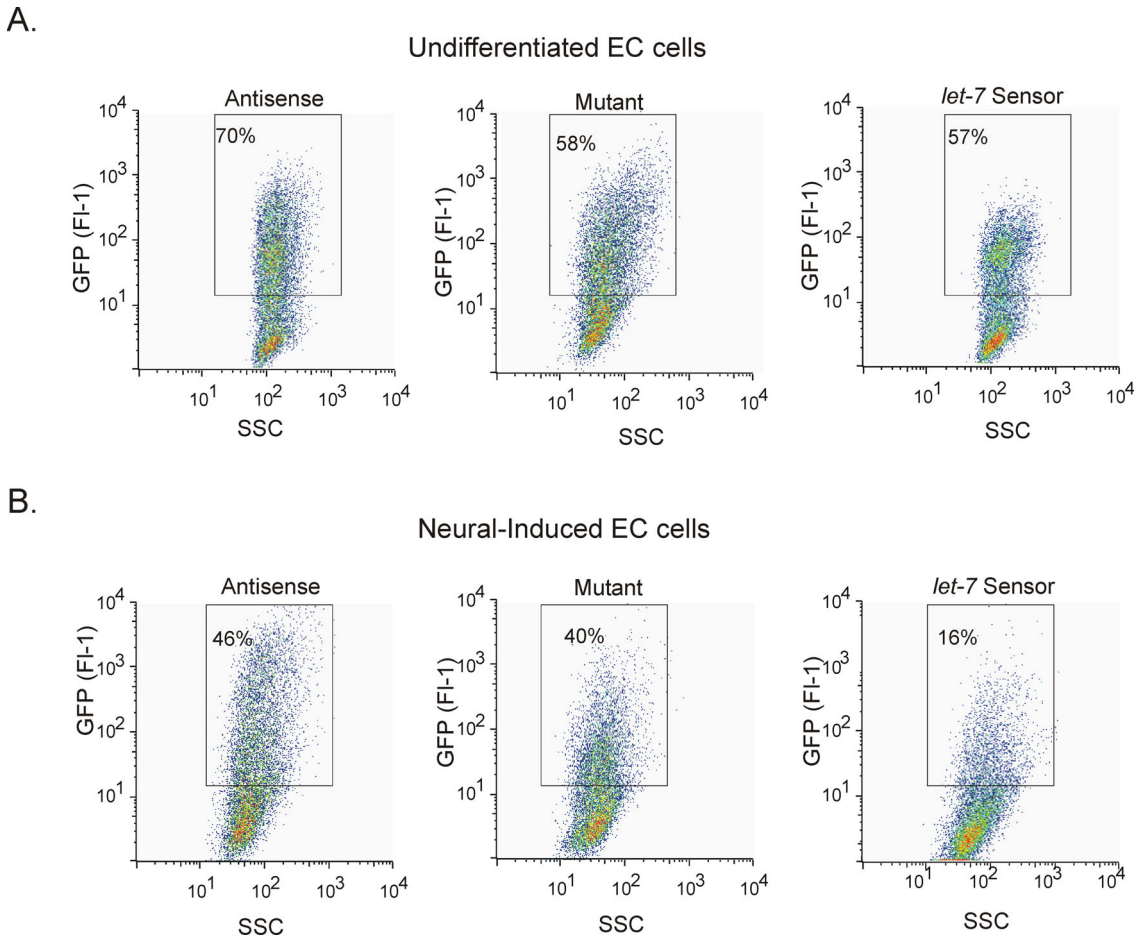

Figure C.37. Representative flow cytometry plots of eGFP expression (GFP Fl-1) versus site scatter (SSC). Gates were established with untransfected cells, for each population the percentage of positive-gated cells is given. EC cell populations stable transfected with peGFP-lin-41 S, antisense control plasmid and mutant control plasmid were assayed prior to (**Panel A**) and 12 days after induction of neural differentiation (**Panel B**).

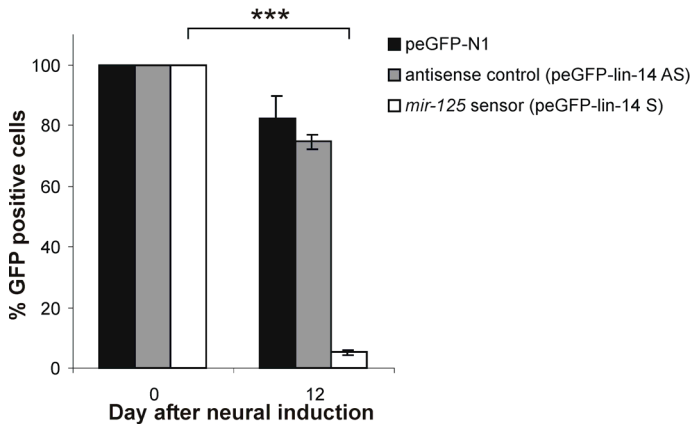

Figure C.38. Quantitative analysis of eGFP expression in EC cells stably transfected with a *mir-125* sensor derived from the *C. elegans lin-14* gene (white bar, peGFP-lin-14 S); the antisense control plasmid (grey bar, peGFP-lin-14 AS); or the parent vector peGFP-N1 (black bar) as indicated to the right. The proportion of $eGFP^+$ cells determined by flow cytometry prior to neural induction was set at 100% and compared to $eGFP^+$ cells 12 days after stimulation with RA. Data are from six independent experiments (n=6, $p<0.001$, Student's paired *t*-test).

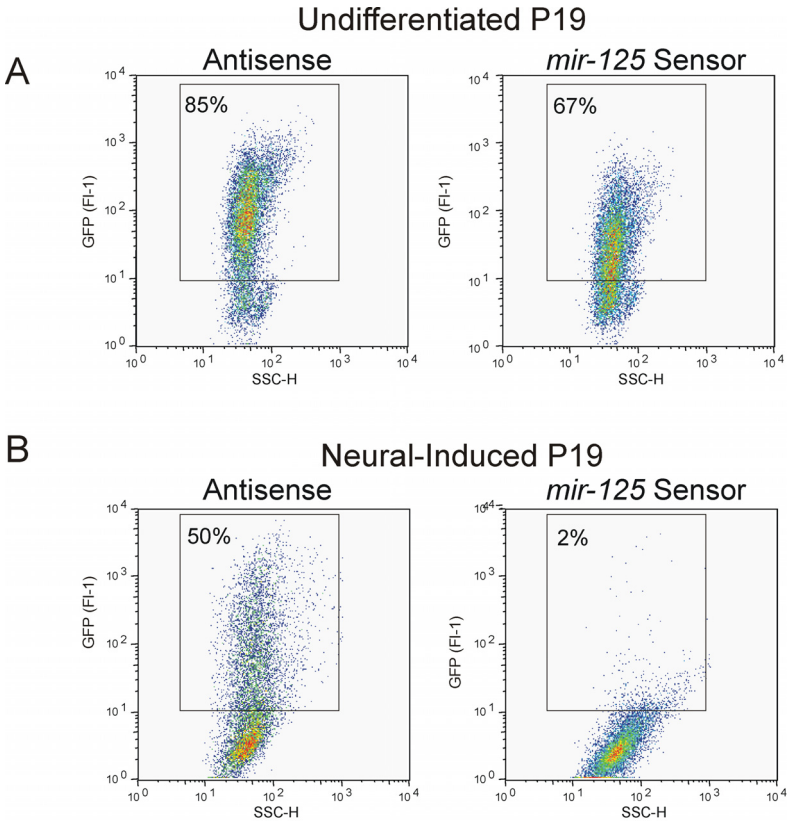

Figure C.39. Regulation of the mir-125 sensor transcript in the course of neural differentiation of P19 EC cells. Representative flow cytometry plots of eGFP expression (Fl-1) versus side scatter (SSC). Gates were established with untransfected cells, for each population the percentage of positive-gated cells is given. EC cell populations stable transfected with peGFP-lin-14 S and antisense control plasmid were assayed prior to (**Panel A**) and 12 days after induction of neural differentiation (**Panel B**).

This data together with the results obtained from primary neurons confirm the lineage specificity of *let-7* and *mir-125* functions. Moreover, these experiments established the reporter assay as an efficient model for the analysis of putative miRNA target genes. The EC assay system allows potential miRNA target genes to be tested in the context of cellular differentiation, and has

the further experimental advantage that it does not rely on ectopic miRNA expression but monitors activity of the endogenous *let-7* miRNA.

C.4.2.4. Downregulation of eGFP mRNA expression after neural differentiation of EC cells containing either let-7 or mir-125 sensor plasmid

Early descriptions of miRNA/mRNA interactions in *C. elegans* support a model in which miRNA act by imperfect binding to the 3'UTR of its target mRNA at the level of translation without affecting mRNA levels [18]. The fate of the *let-7* sensor (peGFP-lin41 S) and antisense control (peGFP-lin41 AS) mRNA was therefore compared during the course of the differentiation protocol by Northern blot (Figure C.40).

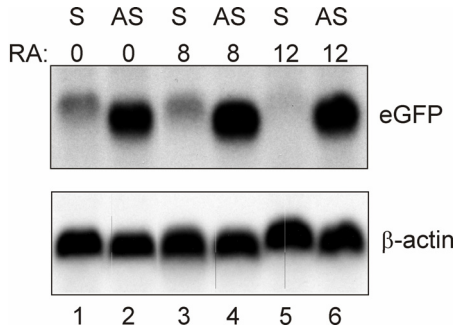

Figure C.40. Northern blot analysis of the *let-7* sensor and control mRNAs during EC cell differentiation. Probes are from the coding region of eGFP shared between sensor (S) and control (C) constructs or β-actin, as indicated to the right. RNA was isolated prior to and 8 or 12 days after stimulation with RA, as indicated above each lane.

Both mRNAs were readily detected in samples from undifferentiated cells (lanes 1 and 2), although the sensor transcript was expressed at markedly lower levels. Nevertheless, both populations contained similar numbers of $eGFP^+$ cells and comparable mean fluorescence (Figure C.34 and Figure C.37). The discrepancy in electrophoretic mobility between the two mRNAs is most likely due to differential use of transcriptional termination signals. In contrast to the results reported in *C. elegans*, downregulation of eGFP expression in sensor-expressing cells is accompanied by the specific loss of the sensor mRNA by Day 12 of the differentiation protocol (Figure C.40, lane 5). Interestingly, at Day 8 sensor mRNA, although falling, was still readily detectable (lane 3). This corresponds to the levels of mature *let-7* miRNA, which at Day 8 are intermediate and rising as determined by Northern blotting (data not shown). Similarly, three fold suppression of sensor expression is also manifest by this time point. Taken together, these results suggest a previously unrecognized complexity in the regulatory interactions between the miRNA and target mRNA.

In contrast to the original descriptions of translational regulation [18], several recent reports have indicated that miRNA may operate at additional levels, including mRNA

compartmentalization, stability and polyadenylation [97,101,102,157,158]. It is important to note that the effect on the *let-7* sensor mRNA levels is independent of promoter or transcriptional termination signals, as these are provided by the vector. Using the EC assay, the same effects have been observed with a sensor derived from a mouse *lin-41* ortholog (see below), as well as a *mir-125* sensor derived from the *lin-14* 3'UTR (Figure C.41). During preparation of this work Bagga et al. also have demonstrated an effect of *let-7* and *lin-4* on *lin-41*, *lin-14* and *lin-28* mRNA degradation in *C. elegans* [159], in contrast to earlier work.

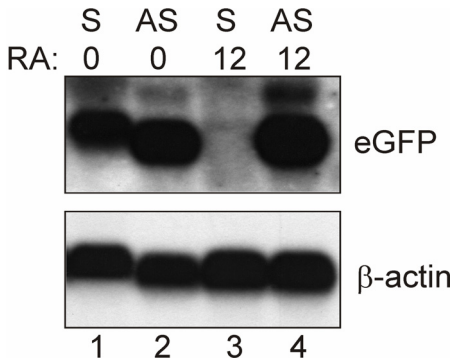

Figure C.41. Northern blot analysis of peGFP-lin14 S and peGFP-lin14 AS control mRNAs during EC cell differentiation. Probes are from the coding region of eGFP shared between sensor (S) and control (AS) constructs or β-actin, as indicated to the right. RNA was isolated prior to and 12 days after stimulation with RA, as indicated above each lane. Notice the loss of *mir-125* sensor mRNA 12 days after neural differentiation.

The results described in Figure C.40 and Figure C.41 suggest that an initial phase of translational repression may serve as a trigger for additional regulatory mechanisms, most likely involving mRNA degradation.

C.4.2.5. Analysis of sensor mRNA stability in EC cells

To better understand the loss of sensor mRNAs during neural differentiation of P19 EC cells (Figure C.40 and Figure C.41), the effect of miRNA expression on target mRNA stability was tested. Undifferentiated (Day 0) or neural differentiated (Day 12) EC cells, transfected with *mir-125* sensor and control plasmid, were treated with Actinomycin D to block new mRNA synthesis. After 0, 0.5, 1, 2, 4, or 8 hours of treatment *mir-125* sensor and antisense control mRNA levels were analyzed by RT-PCR. Primers used in RT-PCR were specific for the open reading frame of the *eGFP* mRNA. As controls, *β-actin* mRNA was taken as a stable mRNA, and *c-Myc* mRNA as an unstable mRNA. In undifferentiated cells, the expression of the *mir-125* sensor mRNA did not differ significantly from the antisense control mRNA over the course of Actinomycin D treatment (Figure C.42 A). In contrast, 12 days after differentiation the sensor mRNA was destabilized and displayed a significantly reduced half-life compared to the antisense control mRNA (Figure C.42 B). *β-actin* and *c-Myc* mRNA turnovers were similar in both cell populations.

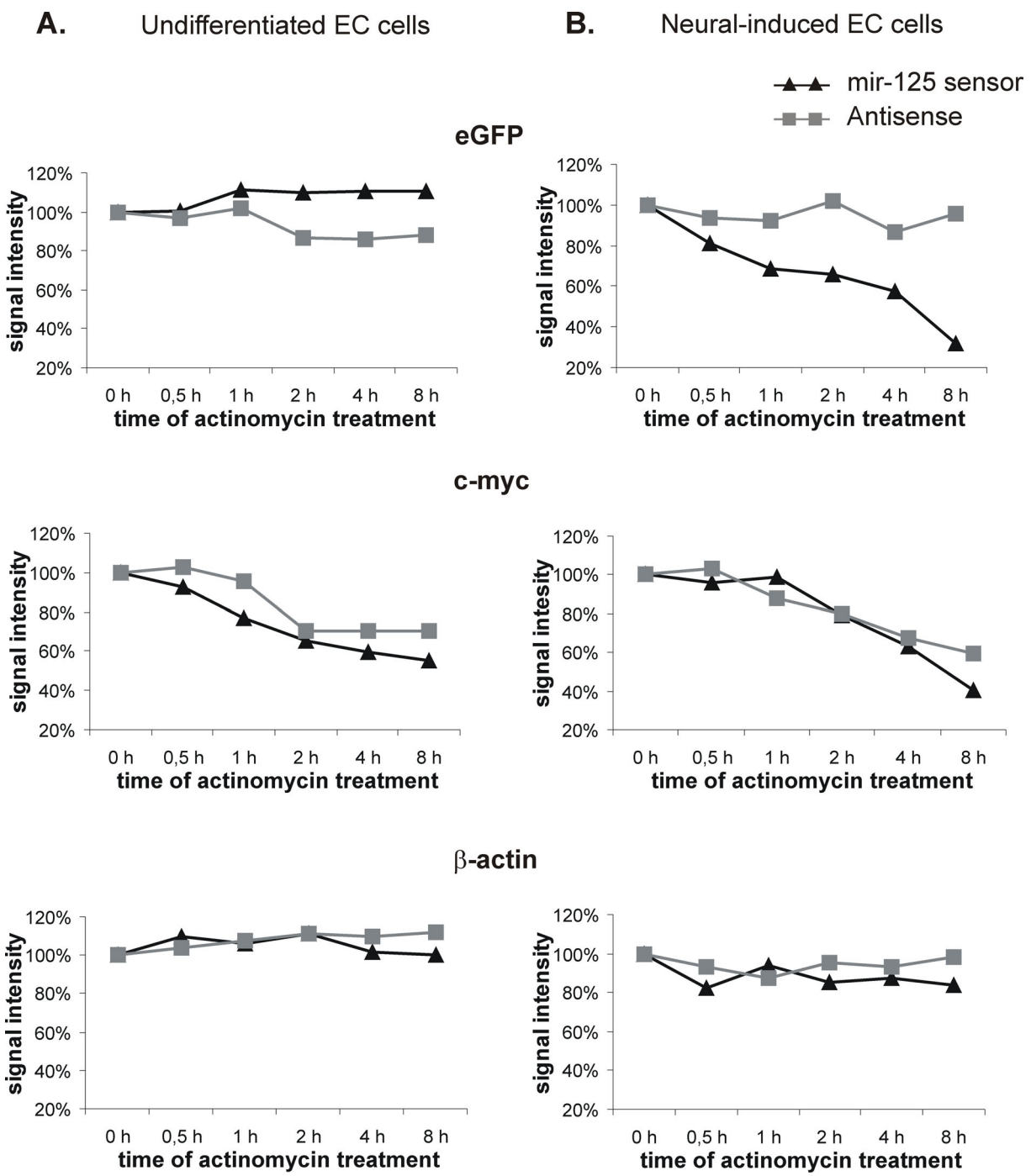

Figure C.42. Analysis of mRNA stability in EC cells. **Panel A**: Undifferentiated EC cells stable transfected either with peGFP-lin14 S (*mir-125* sensor) or peGFP-lin14 AS (Antisense control) were treated with Actinomycin D for different period of time from 0 to 8 hours; target mRNA expression (*eGFP*) was analyzed by RT-PCR. c-*Myc* and *β-actin* mRNAs were analyzed in parallel as controls. The quantification of agarose gel electrophoresis has been done with the ImageJ software. mRNA expression in control untreated cells (time point 0 on the graph) was set at 100%. In **Panel B** the same experiment has been done as described in Panel A, but 12 days after neural differentiation of EC cells.

Two posttranscriptional mechanisms have previously been proposed for downregulation of gene expression by miRNA: mRNA cleavage or translational repression (see Introduction, reviewed in [8]). Briefly, miRNA will specify cleavage if the mRNA has sites with perfect complementarity to the miRNA, sites with imperfect complementarity will lead to translational repression. The results described above demonstrate that mRNA containing imperfect binding sites for either *let-7* or

mir-125 can be targeted for degradation, raising the possibility that regulation at the level of mRNA stability may be more common than previously appreciated for the miRNA pathway. However, it is still unclear by which mechanism miRNAs destabilize the target mRNAs.

C.4.3. A mouse *lin-41* ortholog contains *let-7* binding sites in the 3'UTR

In order to identify mammalian orthologs for the *C. elegans* heterochronic gene *lin-41*, a BLAST search was conducted using the *C. elegans lin-41* sequence to probe the NCBI database. This search identified the closest mouse *lin-41* homolog (which will be referred to as *mlin-41*), initially as a rare expressed sequence tag that was subsequently archived as UniGene Mm.17857. Schulman et al. have found more mammalian *lin-41* orthologs in human, rat, chicken, dog, chimpanzee, and cow [121]. All of the *lin-41* orthologs possess the structural motifs present in members of the NHL family of proteins, a group of RNA-binding proteins involved in the regulation of cell growth and differentiation, including a Ring finger, B-box, a Filamin-type coiled coil, and NHL domains (Figure C.43) [24]. Since the *lin-41* gene has been conserved across phylogeny, it was speculated that the function of this gene in controlling developmental timing is likely to be conserved in mammals.

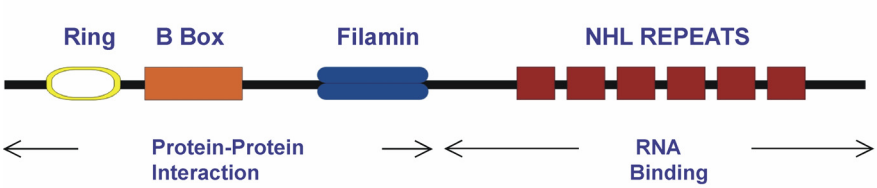

Figure C.43. Key structural domains of LIN-41 proteins and their functions. Ring finger (in yellow), B-box (orange), coiled coil (in blue) domains are characteristic protein-protein interaction domains, the NHL repeats (in red) are an RNA binding domain.

Given the high degree of conservation in miRNA function, the 3' UTR of mouse *lin-41* was manually scanned for potential *let-7* binding sites. Two such sites were identified in close proximity to a potential *mir-125* site (Scheme C.2). Using the strategy from Figure C.25, this cluster of sites was cloned into the peGFP-N1 vector to yield the sensor plasmid peGFP-mlin-41 S. As a control, the two putative *let-7* sites were disrupted by point mutations yielding plasmid peGFP-mlin-41 mut (Scheme C.2).

A.

GGACTTTGGCAACAATCGAATCCTCATCTTCTAATTGTGTCTTCTGGGGTTTTCTGTGTTTA
GGGTGTGCATGTGTGTGTCTCTCATTTTTGAATTTCAAAGAAGAAATCGTCTCAGGGATATT
TCTTTTTCTTTTTCCCCCCCTTTATTTTTATTATTTTTTTTTTTTTAAGAACAAAAGTACAA
CATTGCCTAAGTCCTACCTCAGCTTAAATTTTTTTTTTTTTTTTTTTTTACAGATGAATGT
AATTCTCCTCTGTGCAGGGCTTGAGCCTGTGAAGTGATAATTTCTATCTACCTCAACTCTTT
GCATTTCCCTCTCTGGCAAGCCTCTTGGCTCACATCCTCTTCCCTCCTGAAGGCCTAGGAGG
CACAGGACAGCGGTCCTGCAACCTTGAGGGCACTGGAAGCATATGGTGGGGTGCATGCATTT
TGTAGATTGAGCCAAGGAAACCCAAAAACTACTAAGTAAAAAAGAGAAGTATAAGATGTTGG
AAAGATAGGATTTAAAATTCATAATTGTAGTGTATTTGTGTTCTTGAGAATACTGTG

B.

```
miR-125b      UCCCUGAGACCCU--AACUUGUGA
              ||||||||||||  |      ||||
mlin41        AGGGACUCUGCUAAAGAAGAAACU


let-7a        UGAGGUAG-UAGGUUGUAUAGUU
              |||||||| ||||    ||| ||||
mlin-41       ACUCCAUCUAUCUUUAAUAGUGA
LCS#1


let-7a        UGAGGUAG----UAGGUUGUAUAGUU
              |||||||||    |||||  |||| ||
mlin-41       ACUCCAUCCUGAAUCCGUUACAACAU
LCS#2
```

C.

To disrupt the putative *let-7* sites, two nucleotide exchanges were introduced:

```
let-7a        UGAGGUAG UAGGUUGUAUAGUU
              |  |||||  ||||    ||| ||||
mlin-41       AUUGCAUCUAUCUUUAAUAGUGA
LCS#1

let-7a        UGAGGUAG----UAGGUUGUAUAGUU
              |  |||||    |||||  |||| ||
mlin-41       AAUCGAUCCUGAAUCCGUUACAACAU
LCS#2
```

Scheme C.2. *let-7* complementary sites (LCS) and *mir-125b* complementary site in the 3'UTR of mammalian *lin-41*. **Panel A:** Mouse *lin-41* (Mm.17857; HomoloGene:9076) is defined by the predicted gene XM_356199. Genomic sequence downstream of XM_356199 was examined for miRNA binding sites. Similar clusters are also found in the human (Hs.525846) and rat (Rn.105010) *lin-41* mRNAs. A fragment containing several potential sites was amplified from an undifferentiated P19 EC cDNA library. Primer sequences are underlined; predicted miRNA binding sites are shaded light grey (*mir-125*) or dark grey (*let-7*). **Panel B:** Putative *mir-125b/mlin-41* and *let-7/mlin-41* duplexes from the mouse *lin-41* 3'UTR. **Panel C:** Mutations, introduced in LCSs to disrupt the *let-7* binding.

C.4.3.1. Downregulation of mlin-41 sensor

First, the expression of the *mlin-41* sensor and control plasmids was tested in primary neurons. E15 primary cortical neurons were electroporated with appropriate plasmids as described above for the *C. elegans let-7* sensor. eGFP expression was analyzed 72 hours after transfection. The expression of sensor (peGFP-mlin-41 S) was more than 10-fold lower than the control plasmid in which the putative *let-7* binding sites were disrupted by mutation (Figure C.44). eGFP expression by the double mutant did not differ significantly from the parent vector peGFP-N1.

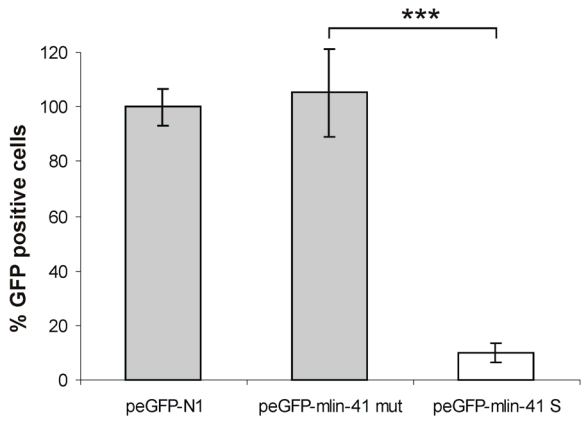

Figure C.44. Regulation of the *mlin-41* sensor transcript in primary neurons. eGFP expression was quantified by flow cytometry. The results are shown for sensor and mutant control plasmid relative to the parent vector peGFP-N1. Grey bars give results for the control plasmids and white bar for the sensor plasmid**.** For each column SEM is indicated. Data are from five independent experiments (n=5, $p<0.001$, Student's paired *t*-test).

These results verify that the two *let-7* binding sites are functional in neurons and that in their absence the mRNA is derepressed. It remains a possibility that *mlin-41* may be regulated by additional miRNAs. The finding that *mlin-41* is regulated by *let-7* is reinforced by the results in EC cells. RA-induced differentiation was accompanied by a five-fold reduction in $eGFP^+$ cell counts in the sensor population (Figure C.45, n=6, $p<0.001$). The expression of eGFP in peGFP-N1 control cell populations was not reduced significantly (Figure C.45, black bar). Interestingly, the mutant control showed also 3.5-fold reduction of eGFP expression after neural differentiation (Figure C.45 grey bar). This effect could be explained by additional regulation of *mlin-41* by other miRNAs and mutations only in *let-7* binding sites are not sufficient to completely derepress the mRNA in EC cells.

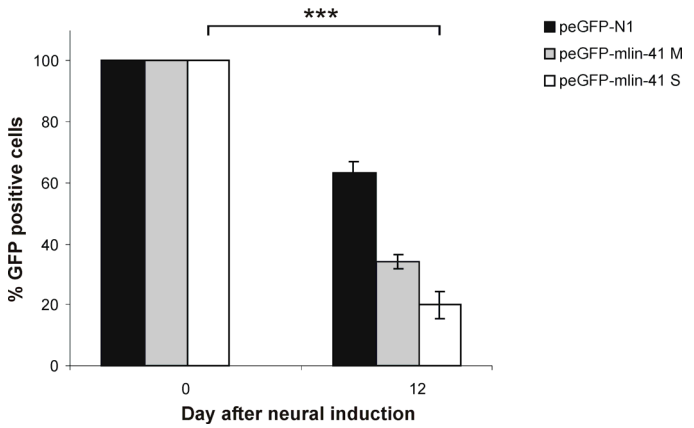

Figure C.45. Regulation of *mlin-41* sensor transcript in the course of neural differentiation of EC cells. eGFP expression was analyzed by flow cytometry at 0 or 12 days of neural induction. The proportion of $eGFP^+$ cells determined by flow cytometry prior to neural induction was set at 100% and compared to $eGFP^+$ cells 12 days after neural induction with RA. Five-fold reduction of sensor (white bar) expression 12 days after RA treatment was observed. Data are from 6 independent experiments (n=6, $p<0.001$, Student's paired *t*-test). Black bar shows the expression of parent peGFP-N1 vector, grey bar mutant control.

As with *C. elegans let-7* and *mir-125* sensors (see Figure C.40 and Figure C.41), examination of the *mlin-41* sensor mRNA revealed a strong reduction in mRNA level in the course of neural differentiation. A Northern blot comparing *mlin-41* sensor, mutant *mlin-41* and eGFP mRNA is shown in Figure C.46. The parent vector peGFP-N1 mRNA was expressed at nearly constant levels, while the mutant control mRNA expression was stable until Day 8 and then was slightly reduced 12 days after neural differentiation (compare lanes 2, 5 and 8). In contrast, the *mlin-41* sensor mRNA was strongly reduced at the eighth day and did not recover (Figure C.46, lanes 1, 4 and 7).

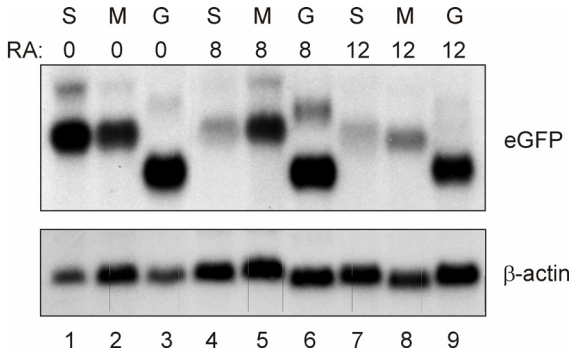

Figure C.46. Northern blot analysis of peGFP-mlin-41 S and control mRNAs during EC cell differentiation. Probes are from the coding region of eGFP shared between sensor (S), control mutant (M) and parent peGFP-N1 (G) constructs or β-actin, as indicated to the right. RNA was isolated prior to and 8 or 12 days after stimulation with RA, as indicated above each lane. Expression of sensor mRNA was strongly reduced after treatment with RA (compare line 1 with lanes 4 and 7). Parent vector peGFP-N1 was stable (lanes 3, 6 and 9). Mutant control was stable until Day 8 (compare lanes 2 and 5), and was reduced after 12 days of RA treatment (lane 8).

C.4.3.2. mlin-41 expression

It has been shown that *let-7* miRNA is temporally regulated during development (Section C.2). In order to investigate whether *mlin-41* is also under temporal control in mammals,

the *mlin-41* and *let-7* expression patterns were compared during mouse brain development and differentiation of EC cells. It was found that *mlin-41* and *let-7* displayed reciprocal expression patterns in the developing mouse embryo and in the course of EC cell neural differentiation (Figure C.47). The expression of *mlin-41* mRNA and protein was detected in undifferentiated EC cells, but not in differentiated cells (Figure C.47 Panel A). In a reciprocal fashion, *let-7* expression was first detected 12 days after neural differentiation of EC cells (Figure C.47 Panel B). During mouse brain development, *mlin-41* mRNA was detected in embryonic stages was decreased at postnatal day 0 and at later developmental times was undetectable (Figure C.47 C). In contrast, the expression of *let-7* miRNA was low until E14, increased until E17 and levelled off thereafter (Figure C.47 D).

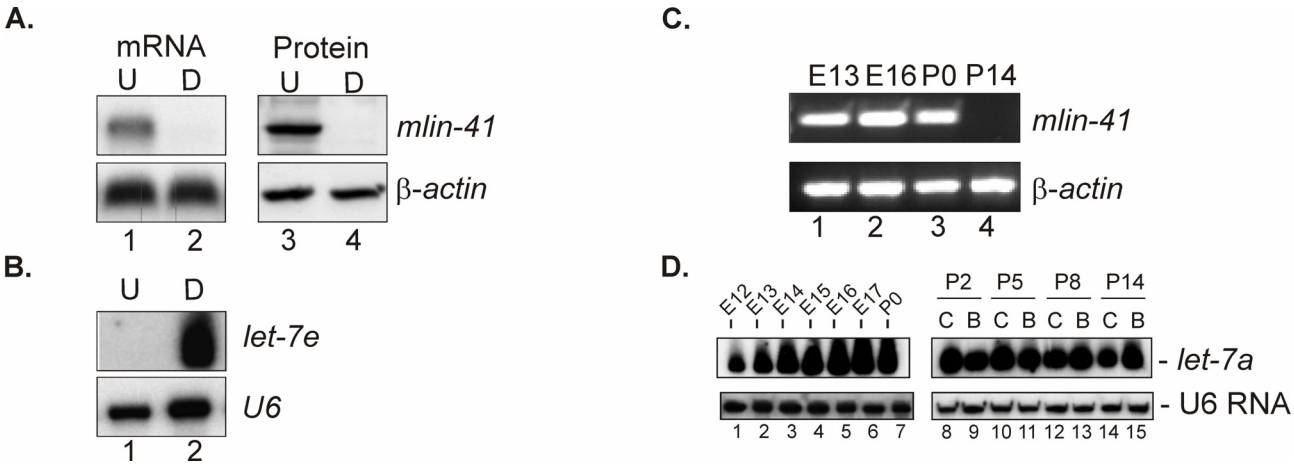

Figure C.47. Reciprocal expression of *let-7* and *mlin-41*. **Panel A:** *mlin-41* expression in EC cells prior to (**U**) and 12 days after stimulation with RA (**D**). Northern blot of total RNA probed for *mlin-41* and as a control for *β-actin* (**Lanes 1** and **2**). **Lanes 3** and **4**: Western blot with anti-mlin-41 serum and as a control anti-β-actin mAb. **Panel B:** *let-7* induction during *in vitro* differentiation of P19 EC cells. Total RNA was prepared from undifferentiated EC cells at Day 0 (U, **Lane 1**); or 12 days after RA treatment (D, **Lane 2**). U6 RNA is shown as the loading control. **Panel C:** *mlin-41* expression during mouse brain development. RT-PCR was performed on total RNA from selected time points from E13 to P14 (**Lanes 1** to **4**). *mlin-41* was amplified with primers specific for 5'UTR. cDNA integrity was monitored using primers specific for β-actin. **Panel D:** Total RNA was isolated from neural tissue representing embryonic Days 12 to 17 (**Lanes 1-6**) and post-natal Day 0 (**Lane 7**). **Lanes 8** to **15**: miRNA expression during early postnatal development. RNA from the cerebellum (B) was prepared separately from the remaining tissue, including midbrain, basal ganglia and cerebral cortex (denoted C) as indicated above each lane. Developmental stage for each pair P2, P5, P8 and P14 is indicated. The U6 RNA expression is shown in the last panel as controls for equal loading.

Taken together, these results confirm the presence of functional miRNA binding sites in the *mlin-41* mRNA and indicate that the *let-7/lin-41* regulatory circuit is conserved between *C. elegans* and mammals (see Discussion). In addition, the data show that the expression of *let-7* is up-regulated at the time when the expression of *mlin-41*, a proposed target of this miRNA, decreases. The reciprocal expression of pattern exhibited by the miRNA is consistent with a model whereby *let-7* may regulate *mlin-41*.

C.4.4. A genetic strategy for the investigation of miRNA functions

C.4.4.1. Description of squelching strategy

In order to analyze the function of miRNA regulatory circuits a competitive interference (or squelching) strategy has been explored. It was postulated that ectopic overexpression of sensor sequences containing high affinity miRNA binding sites would titrate the miRNA from endogenous mRNAs, resulting in a functional knockdown of the miRNA (Figure C.48).

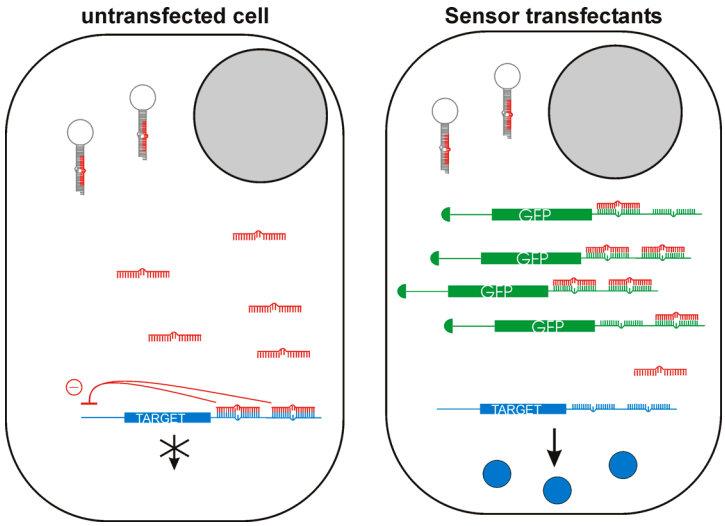

Figure C.48. Carton of competitive interference strategy to knock down the *let-7* function. In untransfected cells, *let-7* (in red) binds to its endogenous target gene (in blue), for example, to mouse *lin-41* homolog, to repress translation of *mlin-41* mRNA and production of mLIN-41 protein. In sensor transfectants, the overexpression of ectopic binding sites on the *eGFP* mRNA (in green) should release endogenous target mRNA (in blue) from *let-7* mediated repression. In this case mLIN-41 protein is produced (blue balls).

As an example, it was speculated that overexpression of the *let-7* sensor mRNA (peGFP-lin-41 S) might interfere with the regulation of endogenous target mRNAs, such as the mouse *lin-41* homolog, by competing for *let-7*. This strategy is particularly suitable for the analysis of miRNA function during stem cell differentiation, as the sensor mRNA is constitutively present throughout the entire differentiation protocol, and in particular the first several days following embryoid body formation when *let-7* accumulation begins.

C.4.4.2. Competitive interference with let-7 promotes differentiation of EC cell-derived astrocytes

For the squelching experiments, sensor and control constructs were generated in the peGFP-N1 vector and also a GFP vector encoding a destabilized form of the protein (yielding pd4eGFP-lin41 S and pd4eGFP-lin-41 AS constructs; see Experimental Procedures) to reduce the possibility that overexpression of eGFP might non-specifically suppress cellular differentiation. For each construct, stable populations of pooled transfectants were obtained by G418 selection and two rounds of sorting for eGFP expressing cells. Differentiation was monitored by

immunocytochemistry with a panel of neuron- and astrocyte-specific markers (Nestin, S100β, GFAP, MAP2, β-III Tubulin, NeuN, A2B5). In the case of GFAP, an increase in GFAP staining was consistently observed after neural induction of *let-7* sensor transfectants compared to control. This result was obtained for both peGFP-lin-41S and the pd4eGFP-lin-41S. Representative plates comparing peGFP-lin-41S and peGFP-lin-41AS are shown in Figure C.49.

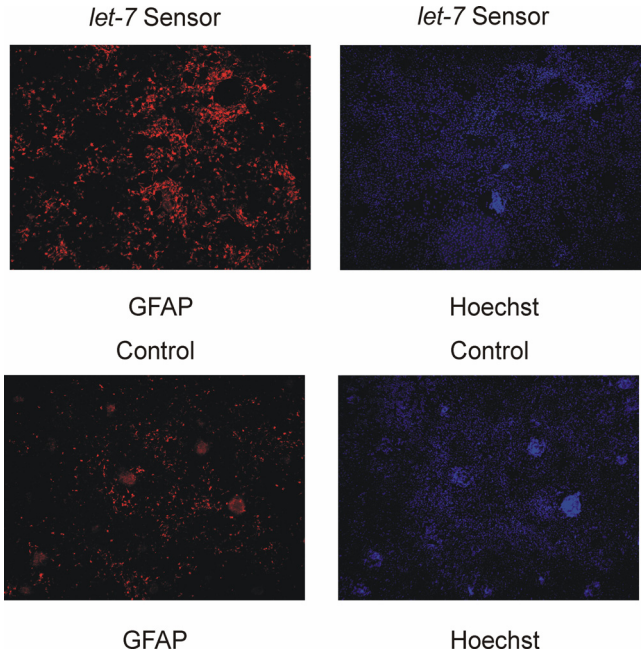

Figure C.49 Immunostaining shows the increase of glial cell number due to competitive interference for *let-7*. EC cells were neural induced with RA and cultivated on cover slips. Cells were fixed and stained on Day 12 after RA stimulation. Sensor transfectants are shown in the upper panel, control transfectants in the lower. Results of indirect immunofluorescence with rabbit anti-GFAP polyclonal antibody (red) and nuclear staining with Hoechst dye (blue) are shown.

GFAP expression in the *let-7* sensor population 12 days after neural induction was also analysed by Western blots (Figure C.50) The control cell population expressed GFAP close to detection limit (lane 4), competitive interference in the sensor population resulted in enhanced GFAP protein expression (lane 3). For comparison, both control and sensor populations expressed similar levels of β-III Tubulin 12 days after neural differentiation.

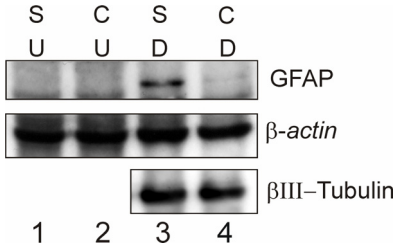

Figure C.50. Western blot analysis of cell lines carrying the *lin-41* sensor (S) or antisense control (C) plasmids. Cell extracts were prepared prior to induction of differentiation (U), or 12 days after neural differentiation (D). Blots were developed with anti-GFAP as well as the neuron-specific anti-β-III Tubulin antibodies, as indicated. Anti-β–actin antibody was used as a control for equal loading. Compare GFAP expression in sensor transfectants (**lane 3**) and control cell population (**lane 4**).

In order to obtain quantitative results, marker expression for the two populations was measured by flow cytometry. Values for the neuronal markers Nestin, β-III Tubulin, MAP2 and NeuN differed by less than 10% between each of the cell populations tested. In contrast, competitive interference with *let-7* in sensor-expressing cells led to an approximately two-fold increase in the expression of the astrocyte-specific marker GFAP. When measured at 10, 12 or 14 days after neural induction, total GFAP-positive cells increased continuously, and sensor transfectants maintained the ~2-fold higher GFAP level at each time point compared to the control (Figure C.51 A).

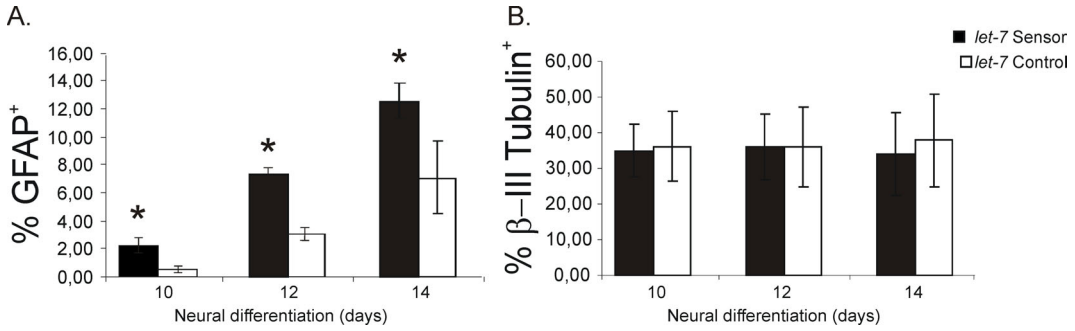

Figure C.51. Summary of flow cytometry data showing time course of astrocyte differentiation (GFAP, **Panel A**) and neuron differentiation (β-III Tubulin, **Panel B**) for lin-41 sensor (black) and control (white) cell populations. Competitive interference with let-7 leads to an increase in astrocyte cell numbers (n=4, $p<0.05$).

Statistical significance was confirmed using the Student's paired *t*-test for each time point (n=4, $p<0.05$). Neuron generation was not affected, as shown for neuron-specific marker β-III Tubulin (Figure C.51 B). Representative flow cytometry plots for the experiment are shown in Figure C.52 A and B.

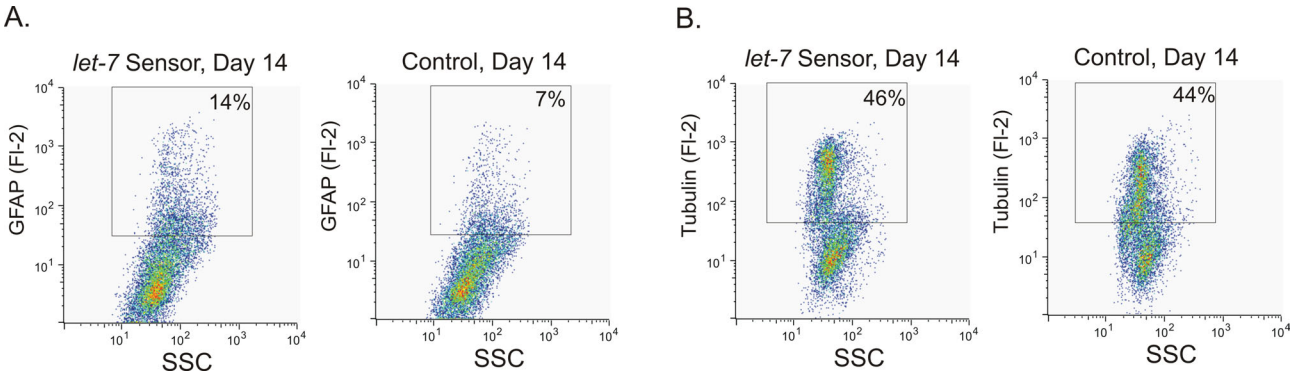

Figure C.52. Representative dot plot of transfected EC cells. Differentiation was monitored by flow cytometry at Day 12 after neural induction using antibodies against GFAP (**Panel A**) and β-III Tubulin (**Panel B**). Gates were established with unstained cells. The percentage of positive cells is given for each diagram.

A second marker for glial progenitor cells, the A2B5 antigen, was evaluated to confirm these results. A2B5 expression was induced during the course of differentiation between Day 6 and Day 11 (Figure B.1). Comparison of *let-7* sensor and control populations revealed an increase in $A2B5^+$ cells of similar magnitude to that observed with GFAP. Results from Day 10 and Day 11 are

presented in Figure C.53 A (n=6, p<0.001). Representative flow cytometry plots are shown in Figure C.53 B.

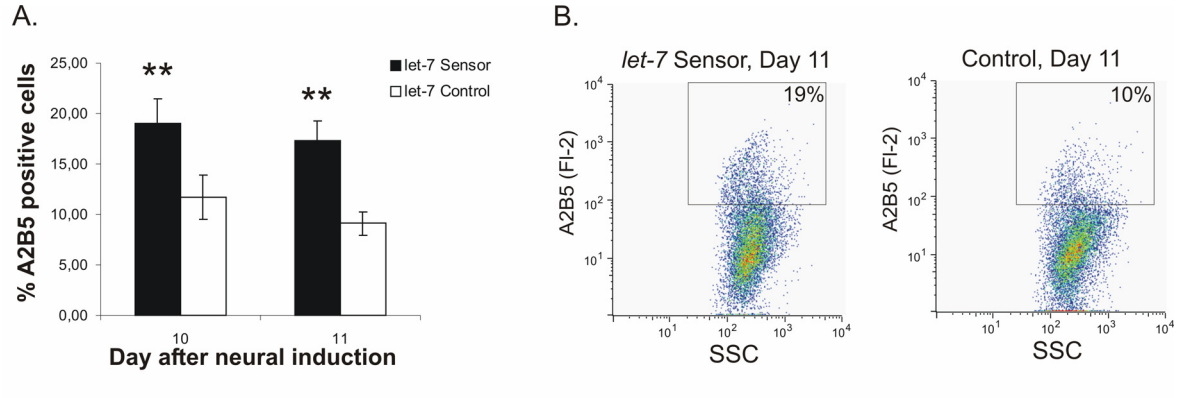

Figure C.53. Competitive interference with *let-7* leads to an increase in glial progenitor cell number. **Panel A:** Summary of flow cytometry data quantifying A2B5 positive astrocyte differentiation for *let-7* sensor (black bars) and control (white bars) cell populations 10 and 11 days after induction of neural differentiation. Unfixed cells were stained with anti-A2B5 mAb. Statistical significance for the A2B5 increase in sensor expression was confirmed using the *t*-test (n=6, p<0.001). **Panel B**: Representative flow cytometry plots of A2B5 positive cells (A2B5 Fl-2) versus side scatter (SSC). Gates were established with unstained cells, for each population the percentage of positive-gated cells is given.

The increase in cells expressing the glial progenitor marker A2B5, as well as the astrocyte marker GFAP in the absence of a commensurate effect on neuronal marker expression suggests that mRNA downstream of *let-7* are involved in gliogenesis. *let-7* is believed to regulate a set of genes involved in cell determination and proliferation. Interference with this pathway leads to an expansion of the astrocytic lineage in the EC cell model.

To determine if endogenous target mRNA are affected by sensor overexpression, the *mlin-41* mRNA was examined by Northern blot. A prominent signal was detected in mRNA from undifferentiated EC cells that was strongly downregulated by Day 4 of neural differentiation in response to RA (Figure C.54). As expected, levels of the *mlin-41* transcript were higher at the onset of the differentiation protocol in cells overexpressing the *let-7* sensor mRNA (compare lanes 1 and 2).

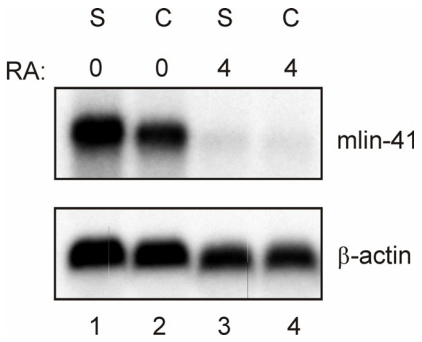

Figure C.54. Northern blot analysis of *mlin-41* and control mRNAs during EC cell differentiation. Probes are from the N-terminus of the *mlin-41* gene or β-actin, as indicated to the right. RNA was isolated from *let-7* sensor (**S**) and mutant control (**C**) transfectants prior to and 4 days after stimulation with RA as indicated above each lane.

Moreover, an effect of competitive interference was also observed on endogenous *mlin-41* mRNA turnover. After treatment of undifferentiated sensor and control EC cells with Actinomycin D, in sensor cells the half-life of the *mlin-41* mRNA was greater than 2 hours, compared to a half-life of under one hour in control cells (Figure C.55). As a control, the degradation of *β-actin* or *c-Myc* mRNAs was comparable in the two cell lines.

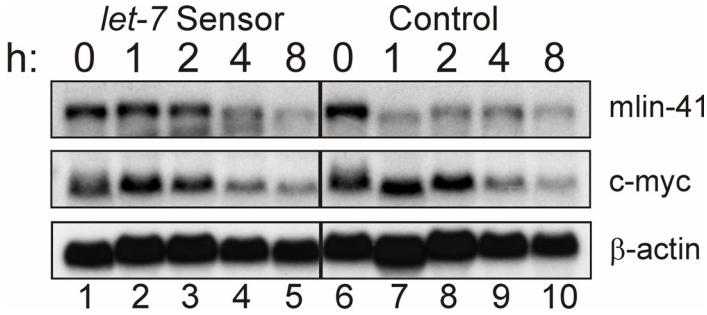

Figure C.55. Analysis of *mlin-41* mRNA stability in undifferentiated EC cells, transfected either with *let-7* sensor construct (**lanes 1** to **5**) or with control mutant plasmid (**lanes 6** to **10**). EC were treated with Actinomycin D for 0, 1, 2, 4, or 8 hours; *mlin-41* mRNA expression was analyzed by Northern blot. *c-Myc* and *β-actin* mRNAs were analyzed in parallel as controls. *mlin-41* mRNA stays more stable in sensor transfectant then in control population (compare lanes 2, 3 with 7, 8).

These observations (Figure C.54, Figure C.55) are consistent with the prediction that at the earliest stages of neural differentiation the *let-7* regulatory pathway can be saturated under the experimental conditions used.

C.4.4.3. Competitive interference with mir-125 promotes differentiation of EC cell-derived astrocytes

The competitive interference strategy was next employed in the functional evaluation of *mir-125* using the *mir-125* sensor. For these experiments, as an additional control an unrelated sensor for the *mir-128* miRNA and its cognate control construct were evaluated in parallel. In the experiment presented in Figure C.56 A, competitive interference with *mir-125* during RA-mediated differentiation of EC cells led to a reproducible, ~2-fold increase in the numbers of GFAP positive cells compared to control transfectants (n=4, p<0,05). Neuron generation was not affected (Figure C.56 B). Furthermore, the effect was specific for *mir-125*, as a squelching construct directed against *mir-128* had no effect. Representative dot plots from one experiment are presented in Figure C.57.

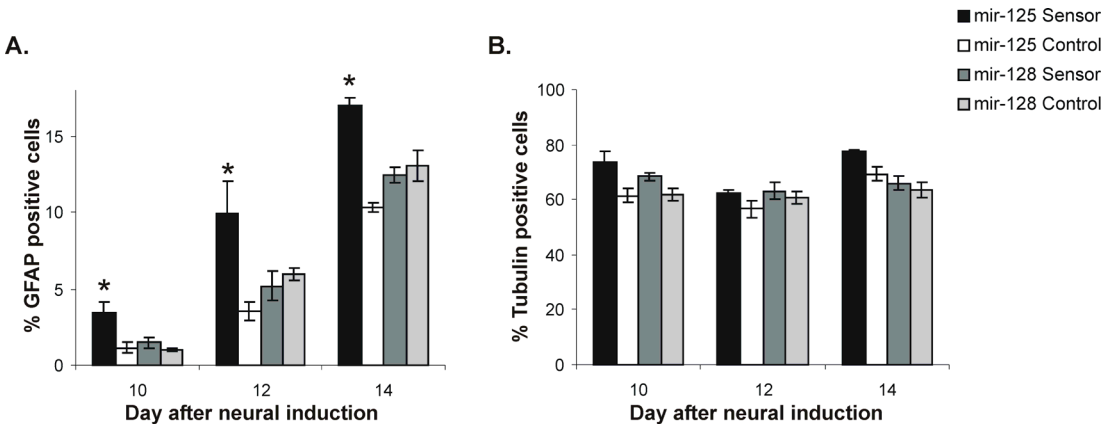

Figure C.56. Competitive interference with *mir-125* leads to expansion of the GFAP positive compartment in the sensor construct (black bars) compared to an antisense control construct (white bars) and to unrelated mir-128 sensor construct (grey bars). Pooled, stable transfectants were treated with RA and assayed for GFAP (**Panel A**) and β-III Tubulin (**Panel B**) expression after 10, 12 and 14 days by intracellular flow cytometry. Each data point represents the sum of four independent experiments. Statistically significant differences are denoted with an asterisk. $GFAP^+$ values for cells transfected with a *mir-128* sensor or control did not differ statistically. Values for the neuronal marker β-III Tubulin differed by less than 10% between each of the cell populations tested.

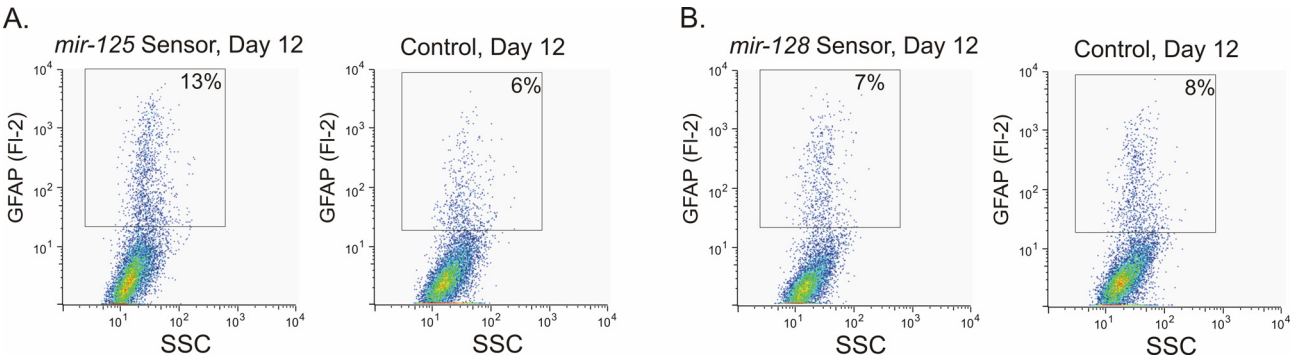

Figure C.57. Representative flow cytometry plots of GFAP positive cells (GFAP Fl-2) versus side scatter (SSC). Gates were established with unstained cells, for each population the percentage of positive-gated cells is given. Cells were fixed and stained with anti-GFAP mAb 12 days after neural induction. **Panel A:** GFAP expansion in *mir-125* sensor transfectants in comparison to the control cell population. As a control for Panel A, GFAP expression in EC cells transfected either with *mir-128* sensor or control plasmids is shown in **Panel B**. There are no differences in GFAP expression between *mir-128* sensor and control transfectants.

These results suggest that the competitive interference assay can be used in the context of stem cell differentiation to screen for miRNA functions in neuro- and astrogenesis. Both *let-7* and *mir-125*, but not *mir-128*, promote astrogenesis using this assay. Additional investigations will be necessary to identify the target genes responsible and to demonstrate their misregulation during a squelching experiment.